iScience

Article

Adenosine deaminase and deoxyadenosine regulate intracellular immune response in *C. elegans*

Graphical abstract

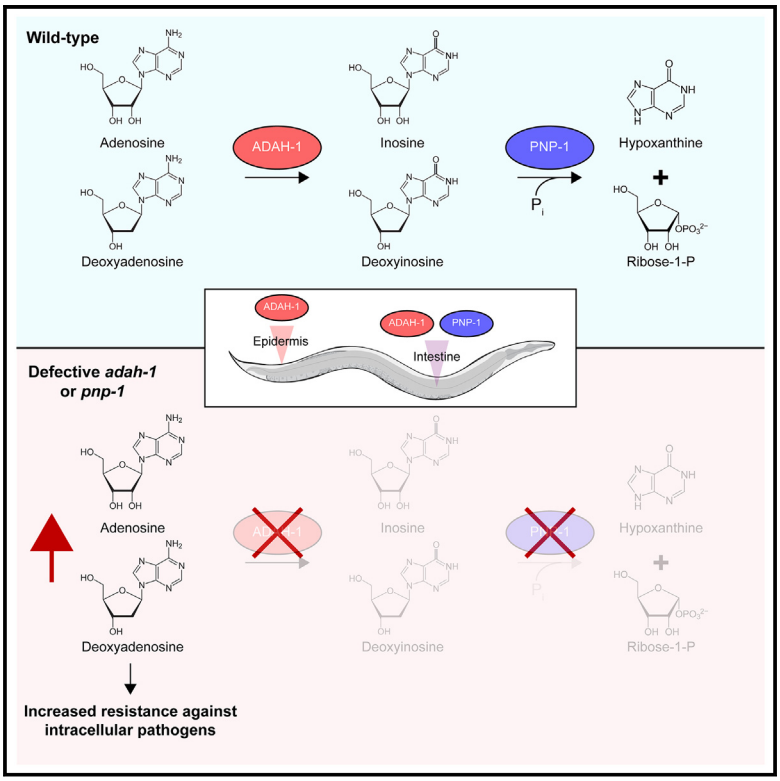

Highlights

- Loss of adenosine deaminase (ADAH-1) induces immunity in *C. elegans*
- ADAH-1 has canonical enzymatic function, converting adenosine into inosine
- ADAH-1 is broadly expressed and functions in intestinal and epidermal cells
- Deoxyadenosine induces immunity in *C. elegans* and in human endothelial cells

Authors

Nicole D. Wernet, Eillen Tecle, Mario Bardan Sarmiento, ..., Damian C. Ekiert, Wendy Hanna-Rose, Emily R. Troemel

Correspondence

etroemel@ucsd.edu

In brief

Immunity; Cell biology; Functional aspects of cell biology.

Wernet et al., 2025, iScience *28*, 111950
March 21, 2025
https://doi.org/10.1016/j.isci.2025.111950

CellPress

iScience

CellPress
OPEN ACCESS

Article

Adenosine deaminase and deoxyadenosine regulate intracellular immune response in *C. elegans*

Nicole D. Wernet,[1] Eillen Tecle,[1,2] Mario Bardan Sarmiento,[1] Cheng-Ju Kuo,[1] Crystal B. Chhan,[1] Ian Baick,[1] Lakshmi E. Batachari,[1] Latisha Franklin,[3] Alice Herneisen,[4] Gira Bhabha,[4] Damian C. Ekiert,[4] Wendy Hanna-Rose,[3] and Emily R. Troemel[1,5,*]

[1]School of Biological Sciences, University of California, San Diego, La Jolla, CA, USA
[2]Department of Microbiology and Immunology, Medical College of Wisconsin, Milwaukee, WI, USA
[3]Department of Biochemistry and Molecular Biology, The Pennsylvania State University, University Park, PA, USA
[4]Department of Biology, Johns Hopkins University, Baltimore, MD, USA
[5]Lead contact
*Correspondence: etroemel@ucsd.edu
https://doi.org/10.1016/j.isci.2025.111950

SUMMARY

Adenosine deaminase (ADA) and purine nucleoside phosphorylase (PNP) are enzymes in the purine salvage pathway, which recycles purines to meet cellular demands. Mutations of these enzymes in humans cause inflammatory and immunodeficiency syndromes, but the mechanisms are not well understood. Prior work in the nematode *Caenorhabditis elegans* demonstrated that loss of PNP ortholog PNP-1 induced an immune response called the intracellular pathogen response (IPR). Here, we show that loss of the enzyme upstream of PNP-1 called ADAH-1 (ADA homolog) also induces the IPR and promotes resistance against intracellular pathogens. Unlike PNP-1, ADAH-1 is essential for organismal development. Importantly, we find that supplementation of deoxyadenosine, a substrate for ADA, induces the IPR and promotes resistance to intracellular pathogens in *C. elegans*, a finding we extend to human cells. Thus, mutations in ADA and PNP induce innate immunity through increased deoxyadenosine, a phenomenon that is conserved from *C. elegans* to humans.

INTRODUCTION

Nucleotides are essential to all life, and thus hosts and pathogens often battle over nucleotide availability during pathogen infection. This battle is particularly important for obligate intracellular pathogens like Microsporidia, which comprise an early branching phylum in the fungal kingdom.[1–3] Notably, microsporidia lack nucleotide biosynthesis pathways and instead use ATP transporters to "steal" host nucleotides while they replicate inside host cytoplasm.[4–6] Similarly, viruses often lack their own nucleotide biosynthetic machinery and thus also rely on host nucleotides in order to synthesize their nucleic acid genomes and transcribe their genes.

To combat viral infection, several host defense pathways deplete the pool of nucleotides. For example, in humans, SAM-domain- and HD-domain-containing protein 1 (SAMHD1) is a nucleotidase that degrades deoxynucleotides needed by human immunodeficiency virus (HIV) for reverse transcription of its genome.[7] Similarly, a recently identified class of ATP nucleotidase effectors conserved between bacteria and eukaryotes cleaves cellular ATP and dATP, which depletes nucleotides and restricts viral replication.[8]

Given the central role of nucleotides and nucleic acids for both hosts and pathogens across organisms, it is perhaps not surprising that they are key regulators of immune responses. When certain types of nucleic acid are found in the eukaryotic cytosol, they serve as triggers of immune responses. For example, viral nucleic acids like double-stranded RNA (dsRNA) or double-stranded DNA (dsDNA) are recognized as "non-self" molecules in the cytosol. Viral dsRNA and dsDNA can be detected by immune sensors like RIG-I-like receptors and STING/cGAS, respectively, leading to induction of the type-I interferon (IFN-I) response, which is a core anti-viral defense pathway.[9] IFN-I genes encode secreted ligands that bind to cell-surface IFN receptors that upregulate IFN-stimulated genes (ISGs), including SAMHD1, to coordinate systemic innate immune responses and clear viral infection.

Although IFN and IFN receptors appear to be vertebrate-specific, recent work in the nematode *Caenorhabditis elegans* has uncovered an immune response pathway in this host that is activated in similar ways to activation of the IFN-I response.[10] This immune response is called the intracellular pathogen response (IPR), and it involves a set of genes induced in common by natural intracellular pathogens of the *C. elegans* intestine such as the Orsay virus and intracellular fungi called microsporidia. *C. elegans* mutants with constitutive IPR expression have increased resistance to both virus and microsporidia infection.[11,12] Similar to RIG-I-like receptors activating IFN-I in response to viral infection in mammals, the RIG-I-like receptor DRH-1 activates the IPR in response to viral infection in *C. elegans*, although the transcription factors used in the IPR and IFN-I response are different.[13] Interestingly, the IPR can be

activated in a systemic manner, which is also a hallmark of the IFN-I response.[14]

Perturbations in purine salvage metabolism are a recently identified trigger common between the IFN-I response and the IPR. Purine salvage enzymes like adenosine deaminase (ADA) act in a pathway conserved from bacteria to humans that is used for recycling purine nucleotides and is more energy efficient than *de novo* synthesis of new purines.[15] Of note, this ADA is an enzyme in the salvage pathway acting on free purines and is distinct from adenosine deaminase acting on RNA (ADAR), an enzyme that acts on nucleic acid and is metazoan-specific, with a separate role in innate immunity.[16] Recently it was shown in endothelial cell culture that small interfering RNA (siRNA) against the human purine salvage enzyme ADA2, which converts the purines adenosine and deoxyadenosine into inosine and deoxyinosine, causes upregulation of IFN-I responses through the accumulation of deoxyadenosine.[17] The *in vivo* relevance of these cell culture findings and their impact on resistance to infection are unclear, and the findings still need to be replicated with ADA2 mutant analysis. Nonetheless, they suggest a possible reason why mutations in human ADA2 cause inflammatory syndromes such as interferonopathies: these mutations may trigger transcription of IFN-I ligands and overexuberant downstream signaling.[18] Notably, increased IFN-I and inflammatory syndromes are also seen in humans with mutations in purine nucleoside phosphorylase (PNP). On the other hand, there are also examples of PNP mutations, as well as mutations in the other human ADA, ADA1, causing immunodeficiency.[19–21] Thus, mutations in multiple purine salvage enzymes cause complex immune system dysregulation, with much to learn about the underlying mechanisms.

In our prior work in the nematode *C. elegans*, we performed an unbiased forward genetic screen to discover negative regulators of the IPR and found the purine salvage enzyme PNP-1 is a negative regulator of the IPR.[22] We demonstrated that loss of *pnp-1* induces IPR gene expression and increases resistance to virus and microsporidia infection. Furthermore, we localized these effects *in vivo* to intestinal epithelial cells, which are key players in *C. elegans* immunity, as these animals appear to lack professional immune cells like macrophages. These findings with *pnp-1* suggested that perturbations in purine metabolites activated the IPR, but it was not clear which other purine salvage enzymes might be involved in this effect, nor was it clear which, if any, purine metabolites may be dysregulated in these mutants to induce an immune response in *C. elegans*.

Here, we find that a previously uncharacterized *C. elegans* gene, *C06G3.5*, encodes an ADA. As such, we named it ADA homolog *adah-1*, and we find it to be a negative regulator of the IPR. Loss of *adah-1*, either by RNAi or by CRISPR-mediated deletion, leads to upregulated IPR gene expression and increased resistance to virus and microsporidia infection. In contrast to *pnp-1*, we find that *adah-1* is an essential gene, as *adah-1* mutants arrest as young larvae. We also find that *adah-1* appears to be expressed in multiple tissues and acts in the intestine to regulate IPR gene expression and resistance to infection. Through testing different purine metabolites regulated by *pnp-1* and *adah-1* activity, we find that deoxyadenosine, a substrate for ADA, induces the IPR and increases resistance to intracellular infection. We also extend these findings about resistance against infection to human endothelial cells. Altogether, our findings indicate that loss of purine salvage enzymes, PNP or ADA, leads to a build-up of the purine metabolite deoxyadenosine, which then activates immune gene expression and pathogen resistance in the *C. elegans* intestine.

RESULTS

The adenosine deaminase ADAH-1 is a negative regulator of *pals-5p::GFP* expression and is essential for larval development

Building on our prior results indicating that the purine salvage enzyme PNP-1 is a negative regulator of the IPR,[22] we performed RNAi knockdown of eight genes predicted to encode other enzymes in the purine salvage pathway to identify which ones might also regulate the IPR (Figures S1A and S1B). We used the *pals-5p::GFP* reporter as a readout for induction of the IPR (*pals-5* is one of the most highly induced IPR genes)[23] and found that RNAi against a previously uncharacterized gene called *C06G3.5* induced *pals-5::GFP* expression, similar to *pnp-1* RNAi (Figures 1A–1C). We named *C06G3.5* ADA homolog *adah-1*, based on its sequence homology with ADAs in other organisms (Figure S1C). ADAH-1 is predicted to be the enzyme acting upstream of PNP-1 in the purine salvage pathway (Figure S1A). Because induction of *pals-5p::GFP* by other IPR triggers like *pnp-1* mutations requires the bZIP transcription factor ZIP-1,[24] we investigated whether the induction of *pals-5p::GFP* by *adah-1* RNAi was dependent on ZIP-1. Indeed, we found that *pals-5p::GFP* was no longer induced by *adah-1* RNAi in *zip-1* mutants (Figure S2A). Therefore, ZIP-1 is required for induction of the *pals-5p::GFP* reporter through loss of *adah-1*, similar to induction by loss of *pnp-1*.

In order to confirm that loss of *adah-1* induces *pals-5p::GFP* expression, we used CRISPR/Cas9 to generate a full deletion of the *adah-1* gene in a *pals-5p::GFP* background, creating the null allele *adah-1(jy125),* which we abbreviate with a "-". Here, we found that *adah-1(−/−)* homozygous mutants arrest during larval development between the first and third larval stage (L1 to L3) (Figures S2B and S2C). Despite arresting during development, *adah-1(−/−)* homozygous mutants showed clear upregulation of *pals-5p::GFP* reporter expression (Figures S2B and S2C). We genotyped and scored the progeny from *adah-1(+/−)* heterozygous animals to more carefully correlate *adah-1* mutant genotypes with *pals-5p::GFP* expression phenotypes and investigate whether this deletion allele was fully recessive. Here, we found that all progeny with *pals-5p::GFP* expression were *adah-1(−/−)* mutant homozygotes, whereas all the animals without *pals-5p::GFP* expression were either *adah-1(+/−)* heterozygotes or *adah-1(+/+)* wild type (Figure S2D). Therefore, deletion of *adah-1* is fully recessive for the phenotype of constitutive *pals-5p::GFP* expression. Because of the developmental arrest caused by the deletion of *adah-1*, we generated an *adah-1(+/−)* heterozygous strain using the *nT1[qIs51]* balancer chromosomal translocation, so the strain could be maintained. Consistent with results described earlier, we found *pals-5p::GFP* induction only in *adah-1(−/−)* mutant homozygotes but not in *adah-1(+/−)* heterozygotes or *adah-1(+/+)* wild-type animals (Figures 1D–1F). Therefore, deletion of *adah-1* appears

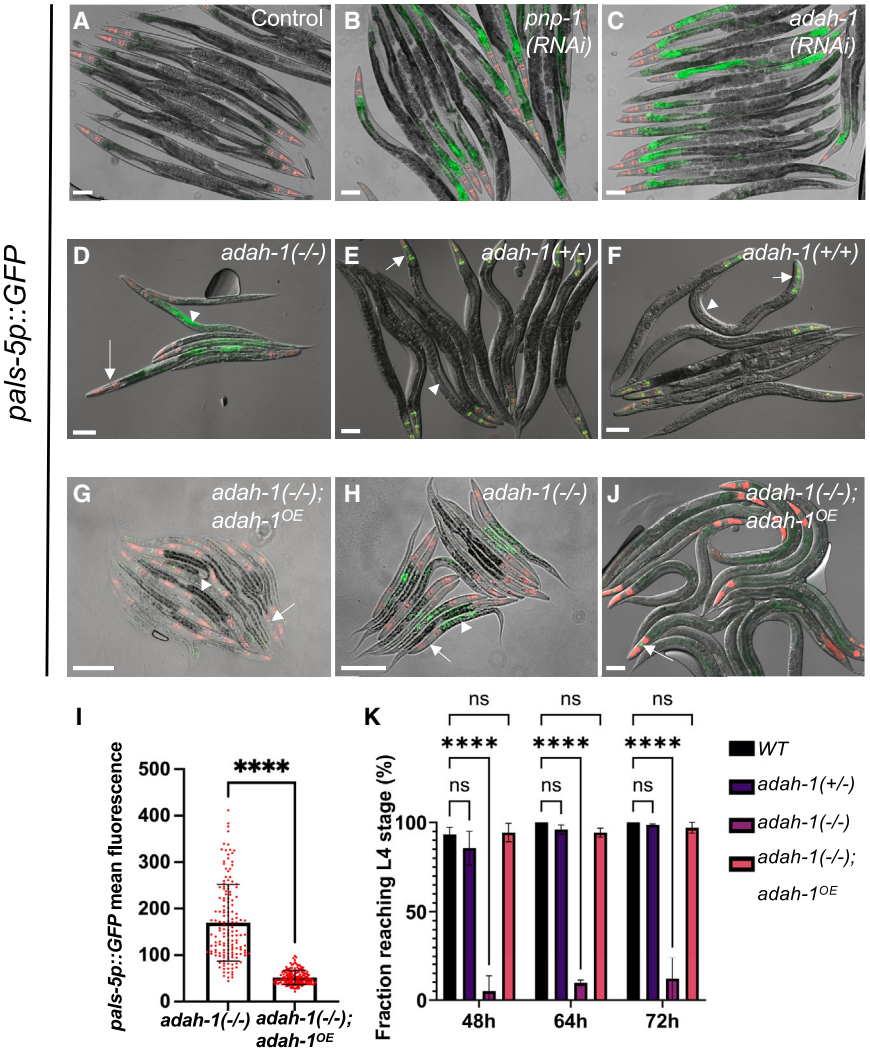

Figure 1. *adah-1* regulates *pals-5p::GFP* expression and is required for larval development

(A–H, J) Animals containing *jyIs8[pals-5p::gfp, myo-2p::mCherry]; pals-5p::GFP* is a reporter for the IPR, and *myo-2p::mCherry* is a marker constitutively expressed in the pharynx, indicating the presence of the *jyIs8* transgene. Scale bars, 100 μm.

(A) Animals treated with L4440 (empty vector control for RNAi), (B) *pnp-1* RNAi, or (C) *adah-1* RNAi. *pals-5p::GFP* is induced in the intestine after *pnp-1* or *adah-1* RNAi compared to L4440 control.

(D–F) Representative images of three genotypes of progeny from the balanced *adah-1(jy125)/nT1* strain. The *nT1* balancer chromosome contains a wild-type *adah-1(+)* allele, and for simplicity, only the *adah-1* genotype is noted in the figure panels with *adah-1(jy125)* noted as "-". (D) *adah-1*(−/−) homozygous mutants can be identified because they lack pharyngeal GFP (arrow) expressed from the *nT1[qIs51]* balancer chromosome, which contains a *myo-2p::GFP* pharyngeal marker. They have constitutively expressed *pals-5p::GFP* expression in the intestine (arrowhead) and arrest as early larvae. (E) *adah-1*(+/−) heterozygotes are also heterozygous for *nT1(qIs51)* and thus have pharyngeal GFP (arrow); they develop into adults and do not exhibit induced *pals-5p::GFP* expression. (F) *nT1/nT1* homozygotes are *adah-1(+/+)*, as indicated by pharyngeal GFP expression (arrow) and the lack of viable embryos at the adult stage, which distinguishes *nT1/nT1* from *nT1/+* heterozygotes. These animals do not exhibit induced *pals-5p::GFP* expression.

(G) *adah-1(−/−)* mutants containing multi-copy extrachromosomal array *jyEx316 [adah-1p::adah-1::mScarlet::3xHA; gcy-8p::GFP]* overexpress *adah-1* and thus are labeled *adah-1(−/−); adah-1*^{OE}. These *adah-1* transgene-containing animals (distinguished by co-injection marker *gcy-8p::GFP* neuronal expression) have lower *pals-5p::GFP* expression compared to (H) their non-transgenic *adah-1(−/−)* siblings, which lack *gcy-8p::GFP* expression and have higher *pals-5p::GFP* expression.

(I) Quantification of *pals-5p::GFP* expression in *adah-1(−/−); adah-1*^{OE} animals shown in (G) and *adah-1*(−/−) mutants shown in (D). Mean *pals-5p::GFP* fluorescence was measured in L1 animals, as *adah-1(−/−)* mutants arrest soon afterward. Three independent experimental replicates were performed, with at least 50 animals per sample. A Mann-Whitney test was used to calculate *p* values; ****$p < 0.0001$. *adah-1(−/−)*^{OE} $n = 152$, *adah-1(−/−)* $n = 160$.

(J) The presence of the *adah-1* transgene is indicated by *gcy-8p::GFP* expression (arrow) and enables *adah-1(−/−)* mutants to develop into adults that do not have *pals-5p::GFP* expression.

(K) Fractions of animals reaching the L4 or adult stage at 48, 64, and 72 h after eggs were laid. WT, *adah-1(−/−) and adah-1(+/−)* animals of the balanced *adah-1(jy125)/nT1* strain, and *adah-1*(−/−)*;jyEx316[adah-1p::adah-1::mScarlet::3xHA; gcy-8p::GFP]* expressing worms (*adah-1*^{OE}). All strains had *jyIs8* in the background. Results are averages of three independent experimental replicates, with 100 animals scored in each replicate at each time point. A two-way ANOVA test was used to calculate *p* values; ****$p < 0.0001$, ns = not significant. Error bars indicate standard deviations (SD).

to cause the fully recessive phenotypes of larval lethality and upregulation of *pals-5p::GFP* expression.

We next sought to rescue the phenotypes of *adah-1(−/−)* null mutants by introducing an extrachromosomal transgene that contains the *adah-1* upstream promoter region fused to the *adah-1a* cDNA, tagged with mScarlet (*adah-1p::adah-1::mScarlet)*. To determine whether this transgene rescues *pals-5p::GFP* expression in *adah-1(−/−)* mutants to wild-type levels, we compared expression levels in mutants with or without the transgene at the L1/L2 stage, because *adah-1(−/−)* mutants arrest around this stage. Here, we found significantly reduced *pals-5p::GFP* expression levels in *adah-1(−/−)* mutants carrying the *adah-1* transgene (*adah-1*(−/−); *adah-1*^{OE}) compared to *adah-1(−/−)* mutants without the transgene (Figures 1G–1I). Furthermore, we found that this *adah-1* transgene rescued the developmental phenotype of *adah-1* mutants, as we found that *adah-1*(−/−); *adah-1*^{OE} animals were able to develop into adults (Figure 1J). Specifically, we found that, in contrast to *adah-1*(−/−) mutants, which arrest before reaching the L4 stage, *adah-1*(−/−); *adah-1*^{OE} animals developed normally, comparable to the wild-type control (Figure 1K). Altogether, these results confirm that animals defective in *adah-1* have increased

pals-5p::GFP reporter levels. Furthermore, they demonstrate that *adah-1* is essential for larval development. Because of these developmental defects of *adah-1*(−/−) mutants, we used *adah-1* RNAi going forward to define the role of *adah-1* in IPR regulation and immunity.

We next investigated *pals-5p::GFP* expression in animals defective for both *adah-1* and *pnp-1*, which canonically act in an upstream/downstream relationship in the purine salvage pathway, a relationship we confirm in *C. elegans* with metabolomics studies described below. First, we show that *adah-1* and *pnp-1* RNAi cause similar increases in *pals-5p::GFP* expression and that *pnp-1* RNAi has less of an impact than a *pnp-1* mutation, consistent with RNAi only causing a partial loss-of-function phenotype (Figure S2E). Next, we performed *adah-1* RNAi in *pnp-1* mutants. Here, we find that *adah-1* RNAi only causes about 1.5-fold increase in *pals-5p::GFP* expression in *pnp-1* mutants, compared to about 2.5-fold increase in *pals-5p::GFP* expression in wild-type animals (Figure S2E). These findings suggest that *adah-1* may have a greater role in IPR regulation than *pnp-1*. Indeed, *adah-1* has a greater role in development compared to *pnp-1*, as described above. Altogether, these findings are consistent with both *pnp-1* and *adah-1* being negative regulators of IPR gene expression, acting in an upstream/downstream relationship.

Transcriptomic analysis demonstrates that *adah-1* knockdown induces IPR gene expression

Given that the studies above relied on the *pals-5p::GFP* reporter to monitor IPR induction, we next investigated endogenous IPR expression after knockdown of *adah-1* to determine whether this treatment causes similar effects as the loss of *pnp-1*, which we previously demonstrated causes increased IPR gene expression.[22] First, we used RT-qPCR to compare gene expression in animals treated with *pnp-1* RNAi or *adah-1* RNAi, relative to the L4440 negative control RNAi. Here, we saw significant reduction of both *pnp-1* and *adah-1* mRNA, respectively, confirming gene knockdown (Figure 2A). Furthermore, we found that both RNAi treatments led to significant induction of *pals-5* and other IPR genes (Figure 2A). These findings with *pnp-1* RNAi are similar to our previous studies with *pnp-1* mutants and indicate that *adah-1* RNAi has a similar impact as *pnp-1* RNAi in terms of inducing mRNA expression of this subset of IPR genes.

We next performed RNAseq to measure transcriptome-wide changes caused by RNAi against *adah-1*. Here, we performed RNAseq on animals treated with *adah-1* RNAi, *pnp-1* RNAi, or the empty vector control L4440. Differential gene expression analysis revealed that 51 genes ($p < 0.05$, no fold-change cutoff) were significantly upregulated in *adah-1*(RNAi)-treated animals compared to the empty vector control, whereas 20 genes were upregulated upon *pnp-1* RNAi compared to the control (Table S2). We then compared these gene sets to the 80 canonical IPR genes (defined as genes upregulated both by microsporidia *Nematocida parisii* and in mutants for *pals-22*, another negative regulator of the IPR).[11] Here, we found that 34 of 51 upregulated genes in *adah-1* RNAi-treated animals and 16 of 20 upregulated genes in *pnp-1* RNAi-treated animals overlap with IPR genes (Figure 2B, Table S2). In addition, we compared the genes upregulated upon *pnp-1* or *adah-1* RNAi treatment with the genes upregulated in *pnp-1*(*jy90*) mutants and found that all the genes upregulated in the *adah-1* and *pnp-1* RNAi treated worms are also upregulated in *pnp-1*(*jy90*) mutants (Figure 2C, Table S2).[22] Furthermore, we compared the genes upregulated by *adah-1* and *pnp-1* RNAi to genes upregulated in *pals-22(jy3)* mutants and found significant overlap (Figure 2D, Table S2). Of note, we identified fewer genes upregulated with *pnp-1* RNAi than in the *pnp-1* mutant (Figure 2C), likely due to RNAi having less impact on gene function compared to a mutation. Nonetheless, these findings indicate that the loss of either *adah-1* or *pnp-1* leads to the upregulation of a similar set of enriched-for IPR genes, suggesting that *adah-1* acts similarly to *pnp-1* as a negative regulator of IPR gene expression.

To characterize the gene classes regulated by *pnp-1* and *adah-1* relative to genes previously shown to be upregulated upon other IPR triggers, we performed gene set enrichment analysis (GSEA) (Tables S3 and S4; Figure 2E). Here, we found that *adah-1* RNAi significantly upregulates genes that are also upregulated in response to the natural intestinal pathogens *N. parisii* and the Orsay virus, as well as genes that are induced by ectopic expression of the RNA1 segment of Orsay virus (Figure 2E).[13,23] Orsay virus RNA1 contains an active form of RNA-dependent RNA polymerase that is sufficient to induce the IPR via the viral RNA sensor DRH-1/RIG-I.[13] Furthermore, *adah-1* RNAi upregulates genes that are upregulated by other IPR triggers like the proteasome inhibitor bortezomib and heat stress, as well as in *pnp-1* and *pals-22* mutants (Figure 2E). Overall, these results highlight the role of the purine salvage enzyme ADAH-1 as a negative regulator of the IPR, acting similarly to the previously characterized purine salvage enzyme *pnp-1* in its effects on gene expression.

Metabolomic analyses indicate that ADAH-1 acts as a canonical adenosine deaminase

Next, we investigated whether ADAH-1 functions as a canonical ADA, acting upstream of PNP-1. ADA and PNP are both enzymes of the purine salvage pathway that is conserved from bacteria to humans, with ADA acting upstream of PNP (Figure S1A). Specifically, ADA catalyzes the deamination of adenosine into inosine, and PNP then catalyzes the conversion of inosine into hypoxanthine (Figure 3A). Our previous targeted metabolomic analysis of PNP-1 using liquid chromatography-mass spectrometry (LC-MS) confirmed it likely behaves as a canonical PNP, as we found that *pnp-1* mutants have increased levels of inosine and lowered levels of hypoxanthine compared to wild-type animals.[22] Here, as a positive control for our *adah-1* LC-MS analysis, we again found that *pnp-1* mutants had increased inosine and decreased hypoxanthine levels compared to wild-type animals, as well as increased levels of adenosine (Figure 3B). Then, to investigate the enzymatic activity of ADAH-1, we used RNAi knockdown. Here, we found that RNAi against *adah-1* led to significantly increased levels of adenosine, and decreased levels of inosine and hypoxanthine, as might be expected if ADAH-1 were catalyzing the canonical ADA reaction (Figure 3C). Thus, it appears that ADAH-1 is a bona fide ADA that acts upstream of PNP-1 in the purine salvage pathway.

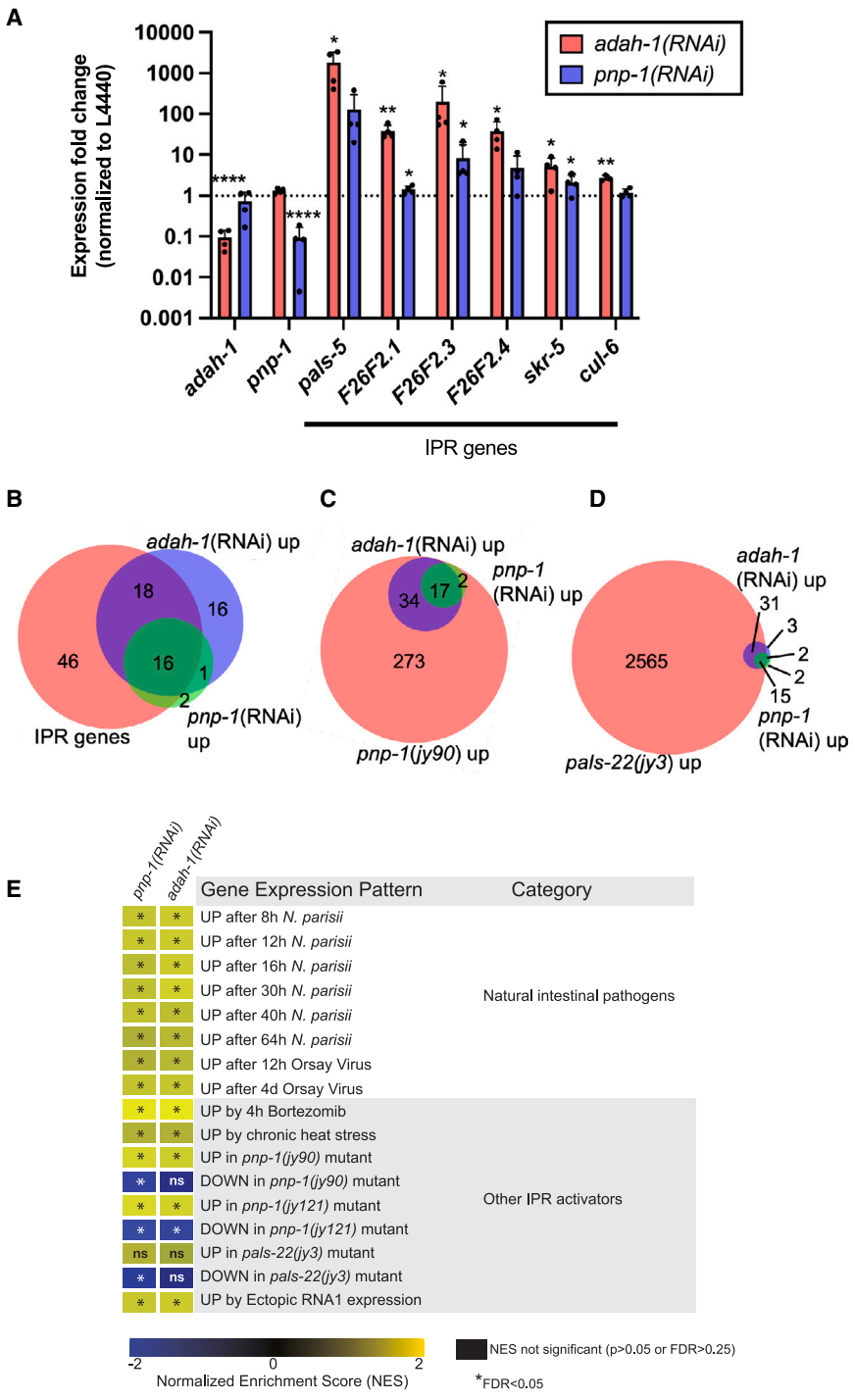

Figure 2. Endogenous IPR gene expression is induced by knockdown of *pnp-1* or *adah-1*

(A) RT-qPCR of a subset of IPR genes in *adah-1* and *pnp-1* RNAi-treated adults. Fold change in gene expression is shown relative to empty vector control. Graphs show the combined results of four independent experiments. An unpaired, one-tailed Student's t test was performed. **p* value <0.05, ***p* value <0.01, ****p* value <0.001, *****p* value <0.0001. (B) Venn diagram comparing gene sets of upregulated genes in *adah-1* and *pnp-1 RNAi*-treated animals, respectively, with 80 canonical IPR genes previously described.[11] There is significant overlap between genes upregulated by *adah-1* RNAi and genes upregulated by *pnp-1* RNAi (17 genes in common, rf = 209; $p < 4.26e\text{-}40$). There is significant overlap between IPR genes and genes upregulated by *adah-1* RNAi (34 genes in common, rf = 102.2; $p < 9.30e\text{-}68$) and between IPR genes and genes upregulated by *pnp-1* RNAi (16 genes in common, rf = 125.4; $p < 3.31e\text{-}33$).

(C) Venn diagram of genes upregulated by *adah-1* RNAi and *pnp-1* RNAi, and genes upregulated in *pnp-1(jy90)* mutants from a previous study.[22] All 54 genes upregulated by *adah-1* RNAi are also upregulated in *pnp-1(jy90)* mutants (rf = 36.5; $p < 3.56e\text{-}82$). All 19 genes upregulated by *pnp-1* RNAi are also upregulated in *pnp-1(jy90)* mutants (rf = 36.5; $p < 1.21e\text{-}30$).

(D) Venn diagram of genes upregulated by *adah-1* RNAi and *pnp-1* RNAi and genes upregulated in *pals-22(jy3)* mutants from previous study.[11] There is significant overlap between genes upregulated by *adah-1* RNAi and genes upregulated in *pals-22(jy3)* mutants (46 genes in common, rf = 4.1; $p < 2.42e\text{-}25$). There is significant overlap between genes upregulated by *pnp-1* RNAi and upregulated in *pals-22(jy3)* mutants (15 genes in common, rf = 3.6; $p < 1.95e\text{-}07$).

(B–D) rf is the ratio of actual overlap to expected overlap where rf > 1 indicates overrepresentation and rf < 1 indicates underrepresentation.

(E) Correlation of genes differentially expressed upon *adah-1* or *pnp-1* RNAi compared to genes differentially expressed by intracellular pathogens (top half of table with white background) and genes differentially regulated by other immune regulators and various stressors (bottom half of table with gray background). Analysis was performed using GSEA 3.0 software, and correlations of genes sets were quantified as a Normalized Enrichment Score (NES). NES values presented in a heatmap. Blue indicates significant correlation of downregulated genes in an RNAi-treated animal with the tested gene set, yellow indicates significant correlation of upregulated genes in an RNAi-treated animal with the tested gene set, and black indicates no significant correlation ($p > 0.05$ or false discovery rate >0.25). * FDR <0.05, ns = not significant.

Deoxyadenosine supplementation induces IPR gene expression

The results above demonstrated there were altered levels of purine metabolites in *adah-1*- and *pnp-1*-defective animals, suggesting that one of these metabolites might regulate the IPR. Therefore, we investigated whether supplementing purine metabolites that are precursors or products of ADAH-1 and PNP-1 activity might regulate IPR gene expression. Of note, ADA and PNP from other organisms act not only on the RNA forms of nucleosides (adenosine and inosine) but also on the DNA forms (deoxyadenosine and deoxyinosine), which are generally found at much lower levels in the cell,[25,26] and unfortunately were below the level

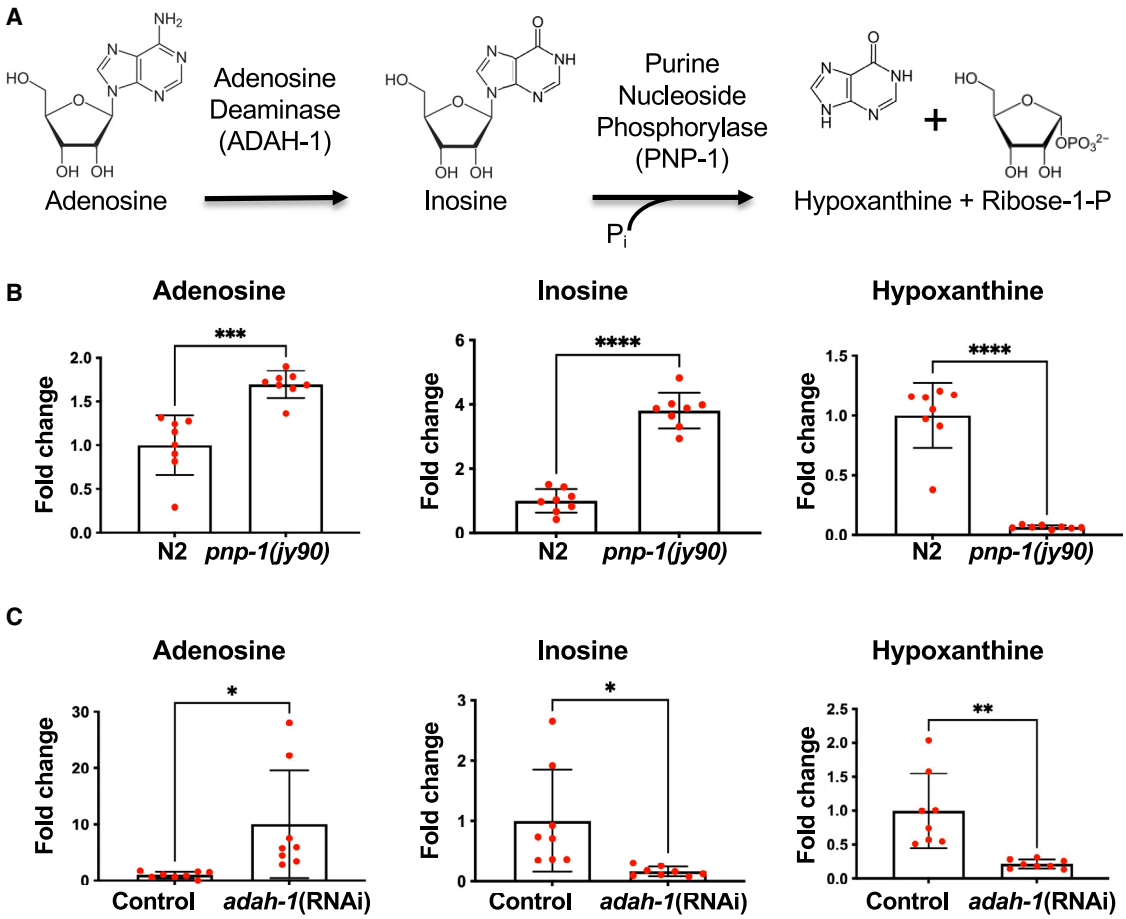

Figure 3. Metabolomics analysis of purine metabolite levels in animals defective for *adah-1* and *pnp-1*

(A) Schematic of reactions catalyzed by ADAH-1 and PNP-1.

(B and C) Quantification of LC/MS analysis of adenosine, inosine, and hypoxanthine levels in different strain backgrounds, showing the mean of eight experimental replicates, each containing one biological replicate per condition composed of thousands of mixed-stage animals. (B) *pnp-1* (*jy90*) mutants have significantly higher adenosine and inosine levels, and lower hypoxanthine levels, compared to wild-type N2 control animals; values were normalized to N2 levels. (C) *adah-1* RNAi-treated animals have increased adenosine levels, and decreased inosine and hypoxanthine levels, compared to control L4440 RNAi-treated animals; values were normalized to L4440 levels. (B and C) Red dots indicate values from individual experiments, and error bars indicate standard deviation (SD). An unpaired t test was used to calculate *p* values; ****$p < 0.0001$; ***$p < 0.001$; **$p < 0.01$; *$p < 0.05$.

of detection in our LC-MS analysis described above. Therefore, we performed dietary supplementation experiments with 30 mM adenosine, deoxyadenosine, inosine, deoxyinosine, and hypoxanthine in wild-type animals and then quantified *pals-5p::GFP* expression. Notably, *C. elegans*' normal laboratory food source of *Escherichia coli* bacteria has previously been shown to interfere with dietary supplementation assays,[27,28] so we used heat-killed *E. coli* as a food source in these assays. Here, we found that supplementation of deoxyadenosine for 24 h caused significant induction of the *pals-5p::GFP* reporter, with adenosine and deoxyinosine having more minor impacts (Figure 4A). We next performed a dose-response curve measuring *pals-5p::GFP* expression upon supplementation with differing concentrations of deoxyadenosine and found increasing *pals-5p::GFP* expression with increasing doses up to 90 mM deoxyadenosine (Figures 4B and 4C). Therefore, deoxyadenosine activates expression of the IPR reporter *pals-5p::GFP*.

Given that 30 mM deoxyadenosine supplementation caused robust induction of *pals-5p::GFP* expression, we used that concentration to further characterize the effects of deoxyadenosine on the IPR. To investigate the impact on endogenous mRNA expression of IPR genes, we performed RT-qPCR after treatment with 30 mM deoxyadenosine and found increased levels of *pals-5* and other IPR genes in comparison to control conditions (Figure 4D). If deoxyadenosine were triggering the IPR similar to other triggers like virus and microsporidia infection, we would expect this induction to be dependent on the transcription factor ZIP-1. Indeed, we found that ZIP-1 was required for the effects of deoxyadenosine, because 30 mM deoxyadenosine supplementation of *zip-1* mutants failed to induce the *pals-5p::GFP* reporter, in contrast to wild-type animals, where deoxyadenosine supplementation induced the *pals-5p::GFP* reporter (Figure 4E). Therefore, deoxyadenosine induces endogenous IPR mRNA expression, which involves the transcription factor ZIP-1.

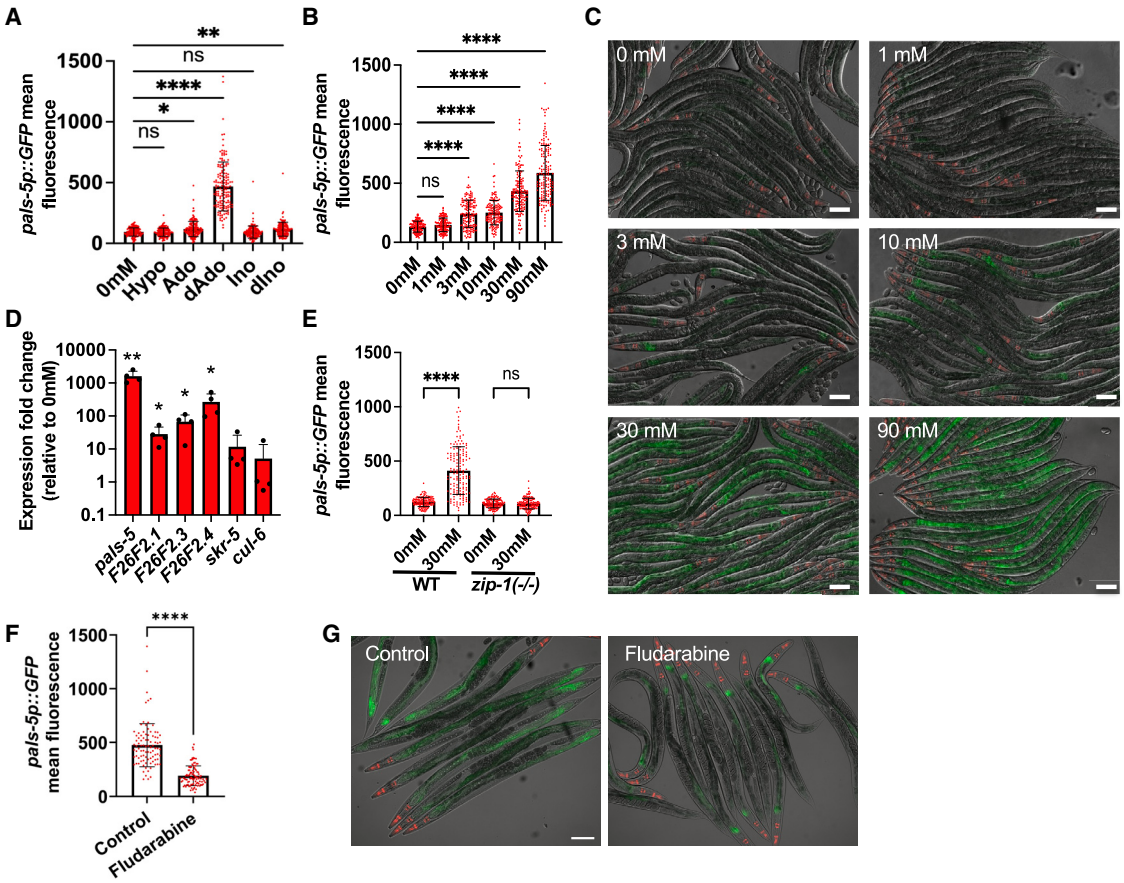

Figure 4. Deoxyadenosine supplementation induces IPR gene expression

(A–C) Treatment of *jyIs8[pals-5p::gfp, myo-2p::mCherry]* animals with various purine metabolites. (A) Quantification of *pals-5p::GFP* fluorescence upon treatment with hypoxanthine (Hypo), adenosine (Ado), deoxyadenosine (dAdo), inosine (Ino), or deoxyinosine (dIno), all at 30 mM, or control (0 mM) for 24 h. Treatment with dAdo caused the most significantly increased *pals-5p::GFP* expression. (B and C) Dose-response curve of *pals-5p::GFP* induction by treatment with different concentrations of dAdo, each for 24 h. Scale bar, 100 μm.

(D) RT-qPCR of a subset of IPR genes upon treatment with 30 mM dAdo for 24 h. An unpaired, one-tailed Student's t test was performed. * p value <0.05, ** p value <0.01; four biological replicates were performed; dots indicate individual replicates.

(E) *pals-5p::GFP* is induced after 30 mM dAdo for 24 h in wild-type animals but not in *zip-1* mutants.

(F) Quantification of *pals-5p::GFP* levels upon treatment of *pnp-1(jy90)* mutants with fludarabine. Treatment for 4 days caused a reduction in *pals-5p::GFP* fluorescence levels compared to a DMSO control. A Mann-Whitney test was used to calculate p values; ****$p < 0.0001$. Control $n = 91$; fludarabine $n = 96$.

(G) Representative images of *pnp-1(jy90)* mutants treated with fludarabine and control (DMSO) after 4 days. Scale bar, 100 μm. (A, B, E) Kruskal-Wallis test was used to calculate p values; ****$p < 0.0001$; ***$p < 0.001$; **$p < 0.01$; *$p < 0.05$; ns = non-significant ($p > 0.05$). Red dots in graphs represent values of individual worms; three independent replicates were performed with $n = 50$ worms each.

To directly test our model that loss of *pnp-1* and *adah-1* induces the IPR due to a build-up of deoxyadenosine, we inhibited the enzyme ribonucleotide reductase (RNR). RNRs are essential for generating DNA building blocks like deoxyadenosine from RNA building blocks.[29] Given that more than one RNR homolog exists in the *C. elegans* genome, we used a pharmacological approach to inhibit RNR, using the drug fludarabine, which is a well-characterized RNR inhibitor.[30] Given the challenges of working with *adah-1* as an essential gene, and the complications of combining drug treatment with feeding RNAi, we focused on *pnp-1* mutants. If IPR induction in *pnp-1* mutants were due to a build-up of deoxyadenosine, we would expect decreased *pals-5p::GFP* expression after drug treatment. Indeed, we found significantly reduced *pals-5p::GFP* expression in *pnp-1* mutants upon fludarabine treatment (Figures 4F and 4G). This finding lends support to the model that build-up of deoxyadenosine in *pnp-1*- and *adah-1*-defective animals is responsible for inducing IPR gene expression.

To further explore the model that build-up of deoxyadenosine is responsible for IPR induction in animals defective for *adah-1* and *pnp-1*, we performed supplementation experiments with 30 mM deoxyadenosine added to *adah-1* RNAi- and *pnp-1* RNAi-treated animals and measured *pals-5p::GFP* expression. Here, we found that deoxyadenosine supplementation caused further *pals-5p::GFP* expression, on top of what was already induced by the RNAi (Figure S3A). This increase may be due to the partial loss-of-function phenotypes caused by RNAi in comparison to a null mutant. Consistent with this model, we did not

find a further increase in *pals-5p::GFP* expression upon deoxyadenosine treatment in *pnp-1* mutants, perhaps due to the stronger phenotype caused by a mutation compared to RNAi (Figure S3B). Alternatively, this lack of effect could be due to the chronic nature of a mutation compared to RNAi treatment, with possible desensitization to the effects of deoxyadenosine. Regardless, these results are consistent with the model that build-up of deoxyadenosine is responsible for IPR induction in purine salvage-enzyme-defective animals.

A prior study by Dhanwani et al. used human endothelial cell culture to demonstrate that siRNA knockdown of ADA2 induced the IFN-I response, which was attributed to a build-up of deoxyadenosine,[17] similar to our findings. Therefore, we explored whether RIG-I-like receptors were required for IPR induction through a *pnp-1* mutation or supplementation with deoxyadenosine, as the model in the Dhanwani et al. study proposes RIG-I and MDA5 are important for the effects of purine salvage enzyme defects on IFN-I response. There are two functional RIG-I-like receptors in *C. elegans* called DRH-1 and DRH-3, and our prior work has shown that *drh-1* is required for inducing the IPR upon viral infection but not required upon other IPR triggers like *N. parisii* infection.[13] Here, we made a *drh-1;drh-3* double mutant and then tested whether crossing in a *pnp-1* mutation or performing supplementation with deoxyadenosine was still able to induce the IPR in these animals lacking functional RIG-I-like receptors. In both cases, we found that deoxyadenosine still induced the IPR (Figures S3C and S3D), indicating that RIG-I-like receptors are not required for purine salvage perturbations to induce the IPR in *C. elegans*, in contrast to the findings reported in human endothelial cells.

Resistance to intracellular pathogens is increased both by RNAi knockdown of *adah-1* and by supplementation with deoxyadenosine

We next investigated whether *adah-1* RNAi increases resistance against intracellular pathogens, as this phenotype is associated with IPR induction. First, we measured resistance after infection with the Orsay virus, which is a single-stranded positive-sense RNA virus that naturally infects the *C. elegans* intestine in the wild.[31] Using fluorescence *in situ* hybridization (FISH) staining of Orsay virus RNA, we found reduced pathogen load after *adah-1* RNAi and *pnp-1* RNAi and in *pnp-1* mutants, our positive control (Figures 5A and S4A). Next, we measured resistance to infection after 3 h of infection with the microsporidian pathogen *N. parisii* by quantifying sporoplasms, which are the parasite cells detectable as the first signs of infection in L1 animals[32]; for examples of sporoplasm quantification, see Balla et al.[33] Consistent with prior results, *pnp-1* RNAi and *pnp-1* mutants had lowered pathogen load (Figure 5B).[22] Importantly, we found that *adah-1* RNAi also lowered *N. parisii* pathogen load. These *adah-1* RNAi conditions did not impair larval development (Figure S4B), or feeding rate as measured by accumulation of fluorescent beads in the intestinal lumen (Figure S4C), which is an important control for pathogen infections delivered through feeding. In summary, these findings indicate that *adah-1*-defective animals have increased pathogen resistance, i.e., lowered pathogen load, when infected with natural intracellular pathogens of the *C. elegans* intestine.

Lowered pathogen load can be associated with increased survival upon infection, which is often called pathogen tolerance or disease tolerance.[34] Therefore, we next examined whether knockdown of *adah-1* and *pnp-1* increased survival upon infection. The Orsay virus does not kill *C. elegans*, so we focused on survival upon infection with *N. parisii*, which does kill *C. elegans*.[35] Here, we found that, consistent with prior results,[22] *pnp-1* mutants had increased survival upon *N. parisii* infection (Figure S5). We also found that *pnp-1* RNAi-treated animals had increased survival, although *adah-1* RNAi-treated animals did not, perhaps due to the greater health impacts caused by loss of *adah-1* compared to loss of *pnp-1*. As shown above, *adah-1* is an essential gene, whereas *pnp-1* is not. Thus, it is likely that because *adah-1* RNAi causes lowered general health in the absence of infection, this effect cancels out the benefits of increased immunity, leading to similar survival rates upon infection with *adah-1* RNAi compared to control-treated animals.

Our model posits that the IPR is an immune program that is not active in wild-type, uninfected animals but can be activated either by infection with pathogens like the Orsay virus or *N. parisii* or by loss of enzymes like *adah-1* and *pnp-1*. Given that the IPR is already off in wild-type uninfected animals, we would not expect that overexpression of *adah-1* would decrease the IPR or resistance to infection. Consistent with this model, we found that *adah-1* overexpression does not cause a change in pathogen resistance in wild-type background (Figures S4D and S4E). Of note, this same *adah-1* construct rescues the *adah-1* mutation (Figures 1G–1K), indicating it is functional. In summary, the lack of effect with *adah-1* overexpression in a wild-type background is consistent with the model that the IPR is off under normal, uninfected conditions but can be induced by loss of *adah-1*.

Next, we investigated pathogen resistance after deoxyadenosine supplementation, as this treatment caused IPR gene induction similar to loss of *adah-1*. First, we exposed animals to deoxyadenosine for 24 h, then infected them with Orsay virus and subsequently measured pathogen load with FISH against the Orsay virus RNA. Here, we found significantly reduced Orsay virus load when comparing 30 mM deoxyadenosine supplementation with control-treated animals (Figures 5C and S6A). Next, we examined resistance to *N. parisii*. Specifically, we exposed L4 animals to 30 mM deoxyadenosine for 24 h, then infected with *N. parisii* and then measured pathogen load with FISH staining for *N. parisii* meronts (replicative form of the parasite) 30 h later. Here as well, we saw significantly reduced *N. parisii* pathogen load after supplementation with deoxyadenosine (Figures 5D and S6A). As a control, we showed that there is not a significant reduction in feeding rate with deoxyadenosine supplementation (Figure S6B). Altogether, these results indicate that increased deoxyadenosine levels increase resistance to intracellular pathogens, consistent with the model that increased levels of this purine metabolite are responsible for IPR induction and increased pathogen resistance in *pnp-1*- and *adah-1*-defective animals.

To extend our findings into studies of human infections, we developed a system to investigate microsporidia pathogen load in human cells treated with deoxyadenosine. We used human umbilical vein endothelial cells previously shown to

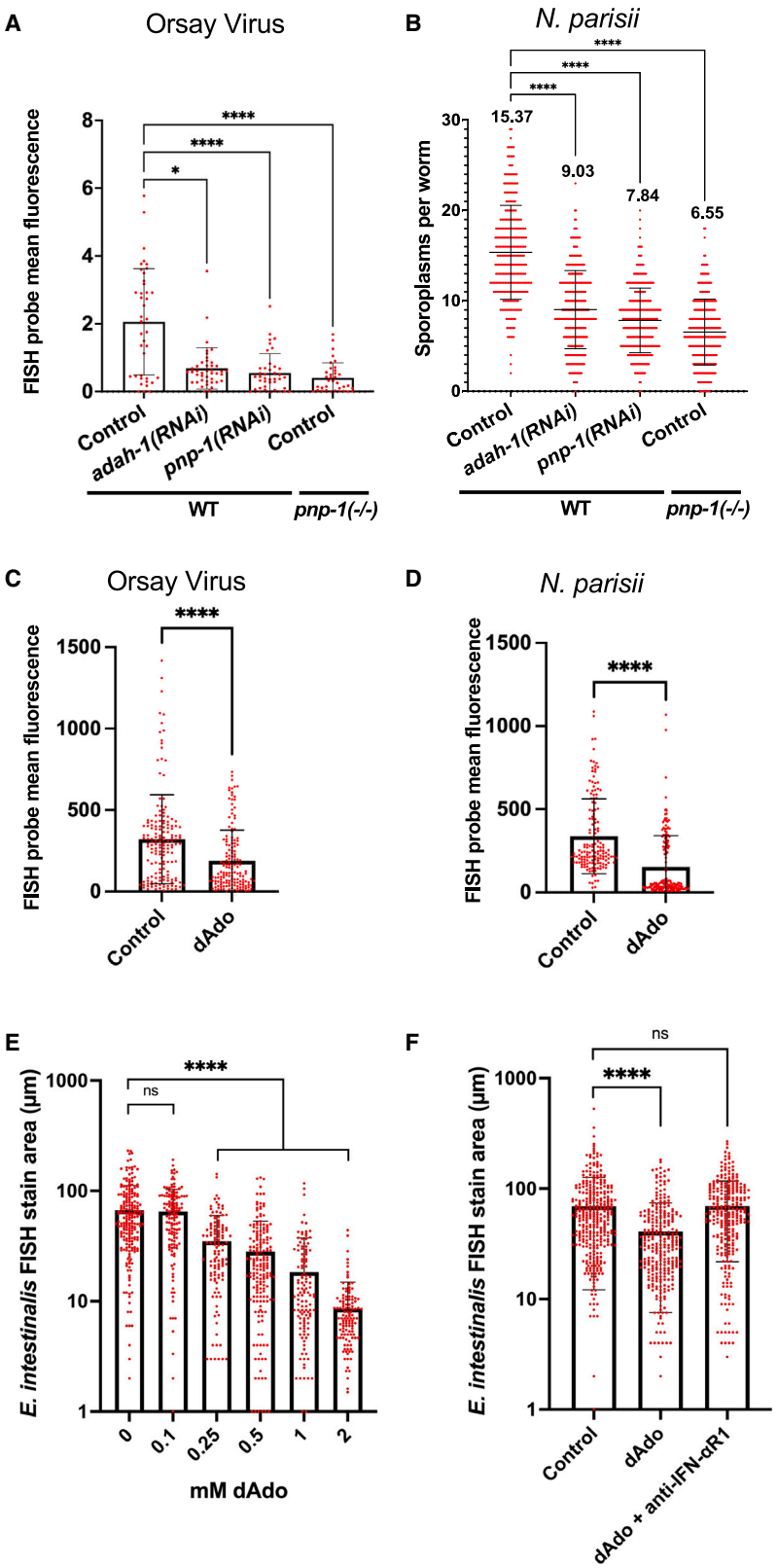

Figure 5. Resistance against intracellular pathogens is increased by *adah-1* knockdown or deoxyadenosine treatment

(A) Quantification of Orsay virus pathogen load at 18 hpi of L4 wild-type N2 animals after being treated with empty vector control RNAi, *adah-1*, or *pnp-1* RNAi, and a *pnp-1* mutant (*jy121*) treated with control RNAi. Infected animals were stained with an FISH probe to label Orsay virus RNA1 and RNA2, and each dot in the graph shows fluorescence for an individual animal across three independent replicates. WT, control $n = 40$; WT, *adah-1*(RNAi) $n = 42$; WT, *pnp-1*(RNAi) $n = 40$; *pnp-1(−/−)* control $n = 36$. Images for quantification were taken with a Zeiss AxioImager; see Figure S4A.

(B) Quantification of *N. parisii* pathogen load at 3 hpi in wild-type animals treated with control, *adah-1*, or *pnp-1* RNAi and a *pnp-1*(*jy121*) mutant treated with control RNAi. Each dot represents the number of sporoplasms for an individual animal; 300 animals per condition were quantified across three independent replicates, with the average sporoplasm number listed at the top.

(C) Quantification of Orsay virus pathogen load 18 hpi determined by mean FISH probe fluorescence in adult *rde-1(ne219)* mutant animals (which are RNAi-defective and thus are more susceptible to infection than wild-type animals) that have been treated with 30 mM deoxyadenosine (dAdo) for 42 h. Control $n = 155$; dAdo $n = 160$. Images for quantification were taken with an ImageXpress plate reader; see Figure S6A.

(D) Quantification of *N. parisii* pathogen load 30 hpi determined by mean FISH probe fluorescence of adult wild-type N2 animals that have been treated with 30 mM dAdo for 54 h. Three biological replicates were performed. Control $n = 164$, dAdo $n = 151$. (A–D) Kruskal-Wallis test was used to calculate p values; $^{****}p < 0.0001$, $^{*}p < 0.05$.

(E) Quantification of *E. intestinalis* pathogen load at 27 hpi after 48 h treatment of human endothelial cells with the indicated concentrations of deoxyadenosine. At least 118 vacuoles were quantified per condition, across three biological replicates.

(F) Quantification of *E. intestinalis* pathogen load at 27 hpi after 48 h treatment of human endothelial cells with 0.5 mM deoxyadenosine and anti-IFNalphaR1 antibody. At least 275 vacuoles were quantified per condition, across three biological replicates. Pathogen load was determined by measuring FISH probe fluorescence area.

induce the IFN-I response upon deoxyadenosine treatment and developed conditions to infect these cells with the pathogen *Encephalitozoon intestinalis*, which is a microsporidian species that causes intestinal infections in humans.[36,37] Prior to infections, we treated these cells with increasing doses of deoxyadenosine, which we found led to decreasing pathogen load, i.e., increasing resistance to *Encephalitozoon intestinalis* (Figures 5E and S4F). To confirm these effects were due to activation of the IFN-I response, we treated cells with an antibody against the IFN-I receptor IFN-alphaR1 and found that the pathogen load increased back to control levels (Figure 5F). In summary, these findings indicate that deoxyadenosine treatment promotes resistance to microsporidia infection in human cells via IFN-I signaling, which is similar to findings that deoxyadenosine treatment promotes resistance to microsporidia infection in *C. elegans* via IPR signaling.

ADAH-1 is expressed broadly and acts in the intestine to regulate IPR gene expression and pathogen resistance

To determine where ADAH-1 is expressed, we analyzed transgenic animals expressing mScarlet-tagged ADAH-1 (using the *adah-1p::adah-1::mScarlet* construct), which rescued *pals-5p::GFP* expression and developmental phenotypes of *adah-1* mutants (Figures 1G–1K). Here, we found ADAH-1::mScarlet expression in multiple tissues throughout the animal including what appeared to be the intestine, the epidermis, neurons, and body-wall muscle (Figure 6A). Due to their morphology, the intestinal cells are easily identifiable. However, other tissues are less so, and thus we confirmed ADAH-1::mScarlet expression in epidermis, neurons, and body-wall muscle by co-localization with GFP reporters expressed in these respective tissues (Figures S7A–S7C). These analyses confirmed ADAH-1::mScarlet expression in the epidermis, neurons, and muscle, supporting the model that endogenous *adah-1* is expressed in multiple tissues in *C. elegans*.

We next investigated in which tissue *adah-1* is required to regulate the IPR. First, we performed tissue-specific RNAi using strains that have the RNAi-deficient *rde-1(ne300)* null mutation, which has less leakiness than the *rde-1(ne219)* partial loss-of-function mutation used in previously described tissue-specific RNAi strains.[38] Using these improved strains, RNAi can be delivered to specific tissues by expressing wild-type *rde-1* specifically in those tissues, such as strain IG1839 that has wild-type *rde-1* expressed specifically in the intestine via *frSi17 [mtl-2p::rde-1 3′UTR] II* and strain IG1846 that has wild-type *rde-1* expressed specifically in the epidermis via *frSi21 [col-62p::rde-1 3′UTR]* (we back-crossed these strains into our N2 strain to generate ERT1265 and ERT1266). Because our prior work has shown the IPR can be induced in the intestine and the epidermis,[14,39] we focused on those two tissues. We treated either wild-type animals, ERT1265, or ERT1266 strains with control, *adah-1*, or *pnp-1* RNAi to perform systemic, intestinal-specific or epidermal-specific RNAi, respectively, and then measured *pals-5p::GFP* expression levels. Our prior studies indicated that intestine-specific expression of *pnp-1* in a *pnp-1* mutant background rescued IPR gene expression and pathogen resistance phenotypes, indicating that *pnp-1* expression in the intestine is sufficient to regulate IPR phenotypes.[22] Here, we saw that RNAi knockdown of *pnp-1* specifically in the intestine leads to increased *pals-5p::GFP* expression, indicating that *pnp-1* expression in the intestine is also required to regulate IPR phenotypes. Furthermore, we found that intestine-specific RNAi against *adah-1* induced the IPR reporter, comparable to systemic knockdown, with *adah-1* RNAi in the epidermis also causing a modest increase in *pals-5p::GFP* expression (Figure 6B). Overall, these findings suggest that loss of *adah-1* in either the intestine or the epidermis will trigger IPR gene expression.

We used these same tissue-specific strains to show that *adah-1* is important in the intestine and epidermis to regulate pathogen resistance. Because the *N. parisii* pathogen resistance phenotype was measured in L1 animals and this stage is too young to see the effects of RNAi, we focused instead on measuring resistance to Orsay virus. Here, we treated wild-type animals with *pnp-1* or *adah-1* RNAi from L1 until L4, then infected them with the Orsay virus followed by FISH staining to quantify viral load. We used wild-type animals as a positive control, as they allow systemic RNAi, and found that, as expected, knockdown of either *adah-1* or *pnp-1* decreased viral load (Figure 6C). Next, we used strain ERT1265 to perform intestinal-specific RNAi and found that knockdown of either *adah-1* or *pnp-1* decreased viral load. Finally, we used strain ERT1266 to perform epidermal-specific RNAi and found a significant decrease in viral load upon *adah-1* RNAi but not upon *pnp-1* RNAi. The requirement in the epidermis for *adah-1*, but not *pnp-1*, expression may be explained by a broader expression pattern of *adah-1* compared to *pnp-1*, which was only seen in the intestine and neurons in our prior study.[22] See discussion for more information on comparing expression of these two genes. Overall, these results indicate that loss of *adah-1* in either the intestine or the epidermis will induce resistance against intracellular pathogens.

Finally, we showed that *adah-1* expression in the intestine is sufficient to regulate the IPR and development, using *adah-1* rescue strains. Specifically, we took the *adah-1* rescue construct and drove expression with either the intestinal promoter *vha-6p* or the epidermal promoter *dpy-7p* and introduced these constructs into *adah-1* mutants. Given that *adah-1* mutants fail to develop, we first needed to assess whether tissue-specific expression of *adah-1* would allow animals to develop. Here, we found that expression of *adah-1* specifically either in the intestine or in the epidermis was sufficient to rescue the developmental defect of *adah-1* mutants (Figure 6D). Next, we measured *pals-5p::GFP* expression in these strains and found again that expression of *adah-1* specifically in either the intestine or the epidermis was sufficient to rescue the increased *pals-5p::GFP* expression of *adah-1* mutants down to near-wild-type levels (Figures 6E and S7D). Thus, *adah-1* expression in either the intestine or the epidermis appears to be sufficient to rescue the developmental defects and the *pals-5p::GFP* expression defects of *adah-1* mutants.

DISCUSSION

ADA and PNP are enzymes in the purine salvage pathway that is conserved from bacteria to humans (Figure S1A). In humans, mutations in these enzymes cause complex syndromes that

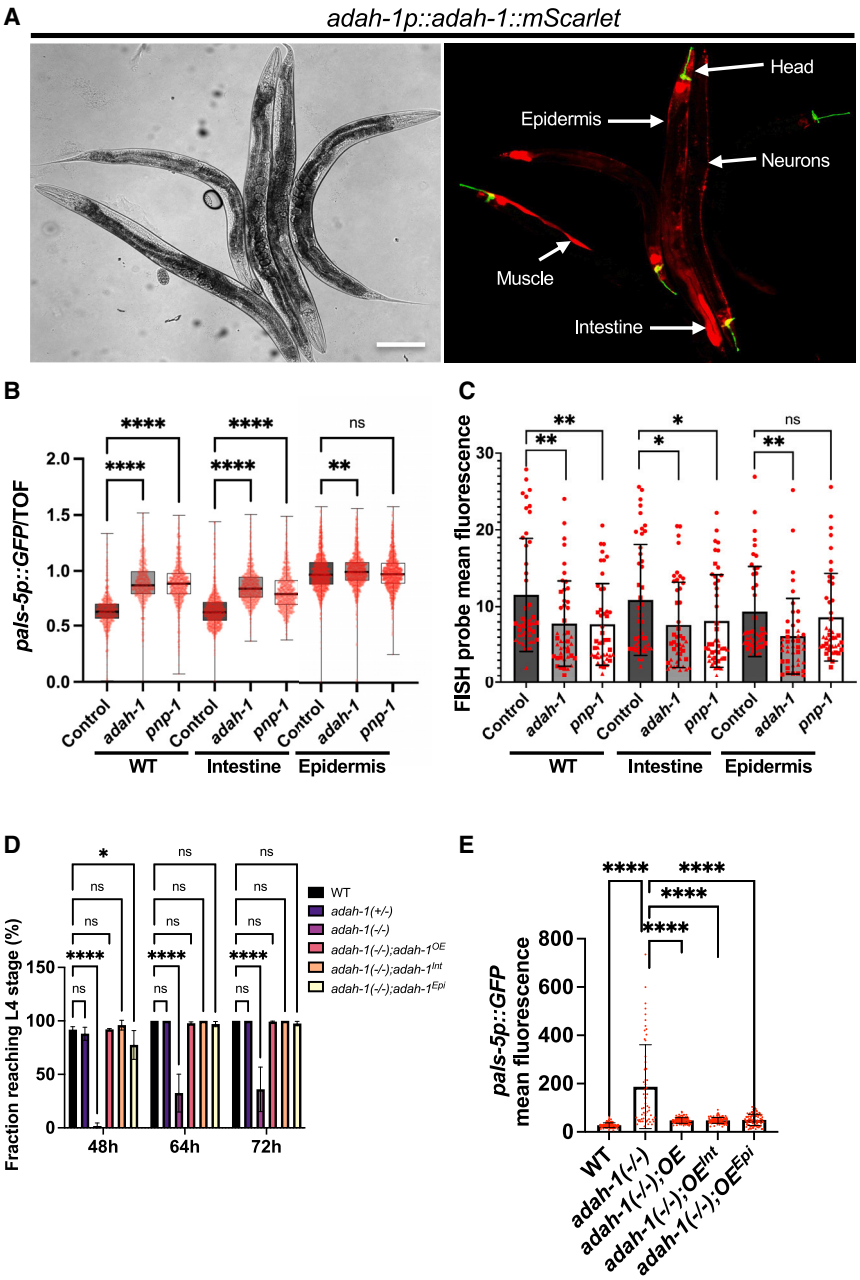

Figure 6. ADAH-1 is required in the intestine to regulate the IPR and pathogen resistance

(A) Expression of *jyEx316[adah-1p::adah-1::mScarlet]*. Arrows indicate expression in different tissues of adult animals. Scale bar, 100 μm.

(B) Box-and-whisker plot of *pals*-5p::GFP expression upon tissue-specific RNAi treatment. GFP expression was analyzed on a worm sorter and normalized to time of flight (TOF, a proxy for length of animals) of *jyIs8* (WT) animals compared to intestinal-specific and epidermal-specific RNAi strains treated with empty vector (control), *adah-1*, and *pnp-1* RNAi. For the epidermis-specific RNAi strain, the overall elevated levels of *pals-5p::GFP* are likely due to the absence of functional *rde-1* in intestinal cells, resulting in impaired transgene silencing and increased baseline expression of the *pals-5p::GFP* transgene. Lines in box-and-whisker plots represent medians, box extends from the 25th and 75th percentiles, and whiskers extend from the box bounds to minimum and maximum values. Red dots indicate individual animals of three independent replicates. A Kruskal-Wallis test was used to calculate *p* values; $^{****}p < 0.0001$, $^{**}p < 0.01$; ns = non-significant ($p > 0.05$). The analysis was performed in three biological replicates. Sample sizes: WT control = 859; intestine control = 1,221; epidermis control = 1,581; WT adah-1 = 750; intestine *adah-1* = 969; epidermis *adah-1* = 1,369; *WT pnp-1* = 984; intestine *pnp-1* = 1,012; epidermis *pnp-1* = 1,259.

(C) Quantification of Orsay virus pathogen load after RNAi treatment with L4440 control, *adah-1*, and *pnp-1* RNAi in wild-type N2 (WT) animals that enable systemic RNAi, as well as intestinal- and epidermal -specific RNAi strains. Mean FISH probe fluorescence of 44–45 animals was quantified across three biological replicates. A Mann-Whitney test was used to calculate *p* values; $^{**}p < 0.01$, $^{*}p < 0.05$; ns = non-significant ($p > 0.05$).

(D) Fractions of worms reaching the L4/adult stage at 48, 64, and 72 h after eggs were laid. Comparison of WT, *adah-1(−/−) and adah-1(+/−)* animals of the balanced *adah-1(jy125)/nT1* strain, *adah-1(−/−);jyEx316[adah-1p::adah-1::mScarlet::3xHA; gcy-8p::GFP]* expressing worms *(adah-1^{OE})*, *jyEx366 [vha-6p::adah-1::mScarlet::3xHA; gcy-8p::GFP]* expressing worms *(adah-1^{Int})*, and *jyEx376[dpy-7p::adah-1::mScarlet::3xHA; gcy-8p::GFP]* expressing worms *(adah-1^{Epi})*. All strains are in a *jyIs8* background. Averages of three independent experimental replicates, with 100 animals scored in each replicate at each time point are shown. A two-way ANOVA test was used to calculate *p* values; $^{****}p < 0.0001$, $^{*}p < 0.05$; ns = not significant. Error bars indicate standard deviation (SD).

(E) Quantification of *pals-5p::GFP* fluorescence in L1 animals of WT animals and *adah-1(−/−)* animals of the balanced *adah-1(jy125)/nT1* strain compared to *adah-1(−/−);jyEx316[adah-1p::adah-1::mScarlet::3xHA; gcy-8p::GFP]* expressing worms *(adah-1^{OE})*, *[vha-6p::adah-1::mScarlet::3xHA; gcy-8p::GFP]* expressing worms *(adah-1^{Int})*, and *[dpy-7p::adah-1::mScarlet::3xHA; gcy-8p::GFP]* expressing worms *(adah-1^{Epi})*. Three independent experimental replicates were performed. A Kruskal-Wallis test was used to calculate *p* values; $^{****}p < 0.0001$. *adah-1(−/−)^{OE}* $n = 118$, *adah-1(−/−)* $n = 58$, *adah-1^{Int}* $n = 120$, *adah-1^{Epi}* $n = 98$. Representative images shown in Figure S7D.

involve both immunodeficiencies and inflammation. For example, over 100 different inflammatory-disease-causing ADA2 mutations have been identified.[18,40] Here, we perform the first analysis of ADA in *C. elegans*, a gene we name *adah-1,* which appears to encode a protein with the same enzymatic activity as its human homolog in catalyzing the conversion of adenosine into inosine. We find that loss of *adah-1* causes similar immune phenotypes as loss of the downstream enzyme *pnp-1*, including upregulated immune gene expression and pathogen resistance against intracellular pathogens. Importantly, we identify the build-up of deoxyadenosine as a likely explanation for the common immune phenotypes in *pnp-1*- and *adah-1*-defective

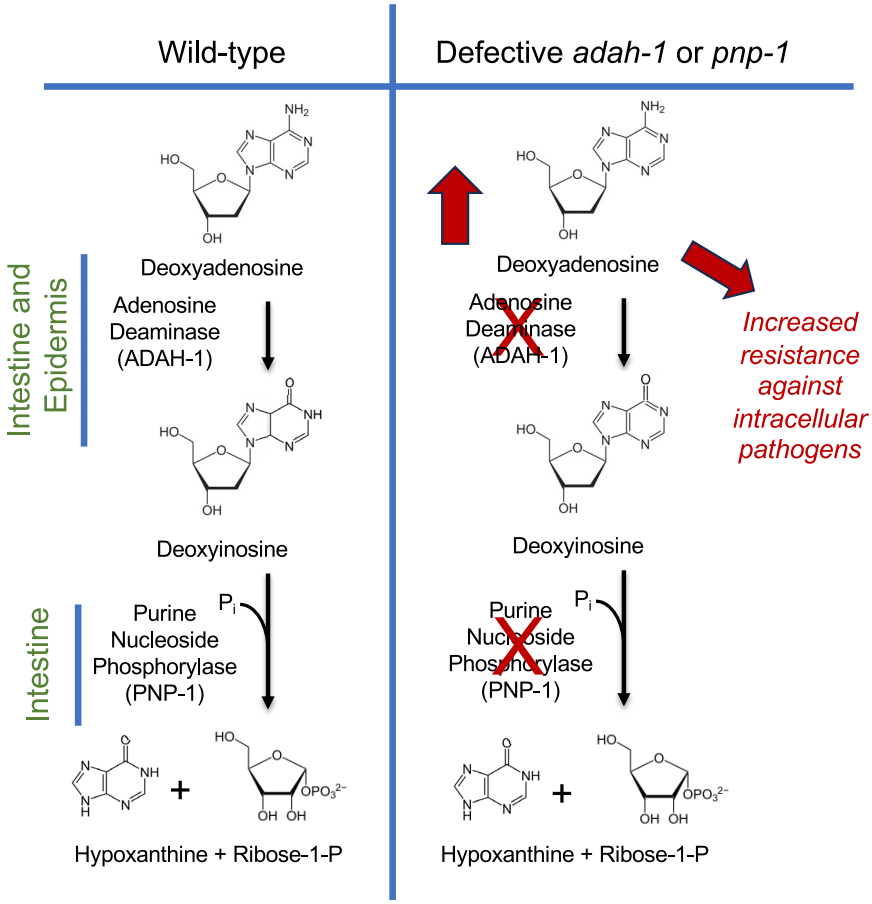

Figure 7. Model of the role of the purine salvage enzymes and deoxyadenosine on intracellular pathogen resistance

animals (Figure 7). We found that supplementation of deoxyadenosine, a substrate for ADA, is sufficient to induce immune gene expression and pathogen resistance in *C. elegans*, a finding we also extended to human cells.

In contrast to the similar immune phenotypes regulated by *adah-1* or *pnp-1*, we found distinct expression patterns for these two genes, with *adah-1* appearing to be expressed in more tissues than *pnp-1* (Figures 6A and S7A–S7C). However, one caveat is that the expression analysis of *pnp-1* used a TransgeneOme construct,[41] which contains about 30 kb genomic region surrounding *pnp-1*, and thus contains more regulatory regions than the cDNA transgene we generated to analyze *adah-1* expression. Therefore, *pnp-1* transgene expression might reflect endogenous gene expression more closely than the expression of the *adah-1* transgene (no TransgeneOme construct exists for *adah-1*). That being said, our tissue-specific RNAi analysis supports the model that *adah-1* is more broadly expressed than *pnp-1*, as immunity was induced by knockdown of *adah-1*, but not by knockdown of *pnp-1*, in the epidermis. The distinct roles for *adah-1* and *pnp-1* indicate they may have distinct roles outside the purine salvage pathway. Indeed, as classic studies of core metabolic pathways expand out from single cells into multicellular organisms, we are learning about potential tissue-specific roles for certain enzymes. For example, recent spatial metabolomics in the model plant *Arabidopsis thaliana* indicate there may be tissue-specific roles for distinct enzymes in the TCA core metabolic pathway.[42] Perhaps there are also tissue-specific roles for distinct enzymes in the purine salvage pathway, as well as transit of intermediate metabolites among those tissues.

In addition to distinct tissue expression patterns, we find that *adah-1* is essential for larval development, whereas *pnp-1* is not. What might account for the larval arrest phenotype caused by loss of *adah-1*, but not loss of *pnp-1*? In addition to the observation that *adah-1* may have broader tissue expression, the major difference we observed in our metabolomics analysis between these two genes was lowered inosine levels in *adah-1*-defective animals compared to increased inosine levels in *pnp-1*-defective animals, as would be expected from their canonical enzymatic functions. Therefore, inosine might be critical for larval development. Alternatively, the developmental defect caused by the absence of *adah-1* might be due to greater build-up of a precursor in *adah-1*-defective animals causing toxicity. Indeed, we saw a more dramatic increase in adenosine upon *adah-1* RNAi than in *pnp-1* mutants (Figure 3). Supporting this model, studies in mammalian cells have demonstrated that mutations in ADA or PNP can cause toxic build-up of adenosine derivatives and T cell death, leading to immunodeficiency.[20] Notably, although we were able to measure adenosine in our metabolomics studies, we were not able to measure deoxyadenosine, perhaps because deoxynucleosides are at low concentrations in non-dividing cells.[25,26] Further metabolomic analyses, together with studies that specifically remove or add different purine metabolites, ideally with tissue-specific precision, might help resolve this question.

Another interesting question for future studies is to investigate why loss of these enzymes, and the resulting putative increase in deoxyadenosine levels, induces immune responses against intracellular pathogens. One possibility is that intracellular infection causes increased levels of deoxyadenosine, either directly or indirectly. For example, obligate intracellular pathogens like microsporidia and *Chlamydia* use ATP transporters to steal host ATP,[43] with *Chlamydia* Npt1 transporter importing ATP, coupled to export of ADP into the host cell.[44] Perhaps activation of such a pathogen-derived transporter causes build-up of cellular ADP, which ultimately is converted into deoxyadenosine. Because obligate intracellular pathogens like *Chlamydia*, microsporidia, and viruses replicate inside the host cell, it would be

necessary to develop spatial metabolomics or other spatially resolved techniques to detect these changes. A separate possibility is that deoxyadenosine levels increase as part of the host response to infection, to trigger further immune responses. For example, in mammalian cells, IFN-I-induced enzyme SAMHD1 serves as a restriction factor for HIV via its ability to degrade host deoxynucleotides, which in turn generates phosphates and nucleosides like deoxyadenosine.[7] Thus, one potential source of deoxyadenosine upon infection could be the by-products of nucleotidases like SAMHD1 acting on dATP reserves, which may serve to deprive obligate intracellular pathogens of the reagents they need to replicate and additionally generate deoxynucleosides to amplify innate immune responses.

A related possibility to explain why deoxyadenosine induces immune responses is that deoxyadenosine might be generated from degrading DNA (i.e., polymerized nucleotides) as a type of damage response. This explanation was proposed to explain findings in human endothelial cells, which similarly to our study, showed that knockdown of an ADA or supplementation with deoxyadenosine induces IFN-I responses in the absence of infection.[17] However, in contrast to *C. elegans* ADAH-1, which appears to be cytosolic, the Dhanwani et al. study in humans was performed with ADA2, which has a signal sequence and is secreted extracellularly (Figure S1C), although a recent report indicates ADA2 may also localize to lysosomes and act on DNA, converting deoxyadenosine to deoxyinosine.[45] In Dhanwani et al., inhibition of ADA2 was proposed to increase extracellular deoxyadenosine, mimicking a break-down product of extracellular DNA, which would serve as a danger signal indicative of tissue damage that can occur during infection,[17] but further work is needed to understand deoxyadenosine signaling in human cells. Notably, cytosolic DNA is also a danger signal, such as when mitochondrial DNA is released into the cytosol,[46,47] which similarly might be degraded to generate deoxyadenosine.

Unlike *C. elegans* and several other organisms that only have one ADA, humans have two ADAs, ADA1 and ADA2. ADA1 lacks a signal sequence and appears to be predominantly intracellular, similar to *C. elegans* ADAH-1 (Figure S1C).[48] Our *C. elegans* studies focused on ADAH-1 in intestinal epithelial cells, and notably, human intestinal epithelial cells do not express ADA2, but instead express ADA1. The role of human ADA1 in regulating IFN-I response is not well understood; instead ADA1 deficiency has long been known to cause profound lymphopenia and severe combined immunodeficiency disease (SCID),[49] in contrast to the ADA2 mutations, which appear to cause mild immunodeficiency and a range of inflammatory phenotypes.[18] Future studies will explore how our *in vivo* characterization of *adah-1* and *pnp-1* in *C. elegans* intestinal cell immunity relate to the complex syndromes seen in humans when ADA1, ADA2, or PNP are mutated and how *C. elegans* ADAH-1 and mouse ADA functions may correspond to human ADA1 and ADA2 functions. Overall, these studies provide new insights into the regulation of immune responses and organismal development by purines, which are critical for all life.

Limitations of the study

Our model posits that loss of *adah-1* or loss of *pnp-1* leads to an increase in deoxyadenosine (Figure 7). Although we were able to detect increased adenosine in animals defective for *adah-1* or *pnp-1*, we were not able to measure deoxyadenosine under any condition, perhaps because deoxynucleosides are at low concentrations in non-dividing cells,[25,26] which are the only type of somatic cell in adult *C. elegans.* Another limitation of our study is that we demonstrated the role of *adah-1* in regulating the IPR in intestinal and epidermal cells, but we did not demonstrate its role in muscle and neuronal cells, where it is also expressed. We do not know the impact of sex or gender in our results. Furthermore, we do not know the mechanism by which deoxyadenosine induces the IPR.

RESOURCE AVAILABILITY

Lead contact

Further information and requests for resources and reagents should be directed to and will be fulfilled by the lead contact, Emily Troemel (etroemel@ucsd.edu).

Materials availability

C. elegans strains generated in this study are available upon request.

Data and code availability

- All data reported in this paper will be shared by the lead contact upon request. RNAseq reads will be publicly available upon publication at NCBI GEO database. Accession numbers are listed in the key resources table. Metabolomics data are available at the NIH Common Fund's National Metabolomics Data Repository (NMDR) Website, the Metabolomics Workbench, https://www.metabolomicsworkbench.org. Accession numbers are listed in the key resources table. The data can be accessed directly via its Project DOI: (https://doi.org/10.21228/M88G2Z).
- This paper does not report original code.
- Any additional information required to reanalyze the data reported in this paper is available from the lead contact upon request

ACKNOWLEDGMENTS

We thank Spencer Gang, Aundrea Koger, Katie Li, Robert Naviaux, Adam Norris, Deevya Raman, Desmond Richmond-Buccola, and Marisa Tsunoda for helpful comments on the manuscript. This work was supported by NIH under R01 AG052622, GM114139, AI176639, and by NSF 2301657 to E.R.T.; by Deutsche Forschungsgemeinschaft (DFG, German Research Foundation) Project 510766555 to N.D.W.; by NIGMS/NIH award K12GM068524 to E.T., by a Postdoctoral Research Abroad Program funded by the Taiwanese National Science and Technology Council grant (109-2917-I-564 -033) to C.-J.K.; by NIH under R35GM128777 to D.C.E.; and by NIH under R01AI147131 to G.B. This publication includes data generated at the UC San Diego IGM Genomics Center utilizing an Illumina NovaSeq 6000 that was purchased with funding from a National Institutes of Health SIG grant (#S10 OD026929). Some strains used in this study were provided by the *Caenorhabditis* Genetics Center (CGC), which is funded by NIH Office of Research Infrastructure Programs (P40 OD010440). Metabolomics data are available at the Metabolomics Workbench, which is supported by Metabolomics Workbench/National Metabolomics Data Repository (NMDR) (grant# U2C-DK119886), Common Fund Data Ecosystem (CFDE) (grant# 3OT2OD030544), and Metabolomics Consortium Coordinating Center (M3C) (grant# 1U2C-DK119889).

AUTHOR CONTRIBUTIONS

Conceptualization, N.D.W., E.T., and E.R.T.; funding acquisition, G.B., D.C.E., W.H.-R., and E.R.T.; investigation, N.D.W., E.T., M.B.S., C.-J.K., C.B.C., I.B., L.E.B., L.F., and A.H.; supervision, G.B., D.C.E., W.H.-R., and E.R.T.; writing—original draft, E.R.T. and N.D.W.; writing—review & editing, N.D.W., E.T., M.B.S., C.-J.K., C.B.C., L.E.B., A.H., G.B., D.C.E., W.H.-R., and E.R.T.

DECLARATION OF INTERESTS

The authors declare no competing interests.

STAR★METHODS

Detailed methods are provided in the online version of this paper and include the following:

- KEY RESOURCES TABLE
- EXPERIMENTAL MODEL AND STUDY PARTICIPANT DETAILS
- METHOD DETAILS
  - RNAi screen of the purine salvage pathway
  - RNAi treatment
  - CRISPR/Cas9-mediated generation of *adah-1(jy125)* mutant, and strain construction with nT1 balancer
  - Generation of transgenic strains
  - Imaging of *C. elegans*
  - *Pals-5p::GFP* expression measurements
  - Developmental rate assay
  - RNA extraction and qRT-PCR
  - RNAseq analysis
  - Functional expression analysis
  - Targeted metabolomics
  - Dietary supplementation of purine metabolites
  - RNR inhibitor treatment
  - Orsay Virus infection
  - *N. parisii* infection, pathogen load quantification and survival assays
  - Bead feeding assay
  - *E. intestinalis* infection and quantification
  - Tissue-specific RNAi
  - Multiple sequence alignment
- QUANTIFICATION AND STATISTICAL ANALYSIS

SUPPLEMENTAL INFORMATION

Supplemental information can be found online at https://doi.org/10.1016/j.isci.2025.111950.

Received: April 11, 2024
Revised: November 22, 2024
Accepted: January 30, 2025
Published: February 3, 2025

REFERENCES

1. Vavra, J., and Lukes, J. (2013). Microsporidia and 'the art of living together. Adv. Parasitol. *82*, 253–319. https://doi.org/10.1016/B978-0-12-407706-5.00004-6.
2. Han, B., and Weiss, L.M. (2017). Microsporidia: Obligate Intracellular Pathogens Within the Fungal Kingdom. Microbiol. Spectr. *5*. https://doi.org/10.1128/microbiolspec.FUNK-0018-2016.
3. Bojko, J., Reinke, A.W., Stentiford, G.D., Williams, B., Rogers, M.S.J., and Bass, D. (2022). Microsporidia: a new taxonomic, evolutionary, and ecological synthesis. Trends Parasitol. *38*, 642–659. https://doi.org/10.1016/j.pt.2022.05.007.
4. Tsaousis, A.D., Kunji, E.R.S., Goldberg, A.V., Lucocq, J.M., Hirt, R.P., and Embley, T.M. (2008). A novel route for ATP acquisition by the remnant mitochondria of Encephalitozoon cuniculi. Nature *453*, 553–556. https://doi.org/10.1038/nature06903.
5. Heinz, E., Hacker, C., Dean, P., Mifsud, J., Goldberg, A.V., Williams, T.A., Nakjang, S., Gregory, A., Hirt, R.P., Lucocq, J.M., et al. (2014). Plasma membrane-located purine nucleotide transport proteins are key components for host exploitation by microsporidian intracellular parasites. PLoS Pathog. *10*, e1004547. https://doi.org/10.1371/journal.ppat.1004547.
6. Major, P., Sendra, K.M., Dean, P., Williams, T.A., Watson, A.K., Thwaites, D.T., Embley, T.M., and Hirt, R.P. (2019). A new family of cell surface located purine transporters in Microsporidia and related fungal endoparasites. Elife *8*, e47037. https://doi.org/10.7554/eLife.47037.
7. Deutschmann, J., and Gramberg, T. (2021). SAMHD1 . and Viral Ways around It. Viruses *13*, 395. https://doi.org/10.3390/v13030395.
8. Rousset, F., Yirmiya, E., Nesher, S., Brandis, A., Mehlman, T., Itkin, M., Malitsky, S., Millman, A., Melamed, S., and Sorek, R. (2023). A conserved family of immune effectors cleaves cellular ATP upon viral infection. Cell *186*, 3619–3631.e13. https://doi.org/10.1016/j.cell.2023.07.020.
9. Rehwinkel, J., and Gack, M.U. (2020). RIG-I-like receptors: their regulation and roles in RNA sensing. Nat. Rev. Immunol. *20*, 537–551. https://doi.org/10.1038/s41577-020-0288-3.
10. Lazetic, V., Batachari, L.E., Russell, A.B., and Troemel, E.R. (2023). Similarities in the induction of the intracellular pathogen response in Caenorhabditis elegans and the type I interferon response in mammals. Bioessays *45*, e2300097. https://doi.org/10.1002/bies.202300097.
11. Reddy, K.C., Dror, T., Underwood, R.S., Osman, G.A., Elder, C.R., Desjardins, C.A., Cuomo, C.A., Barkoulas, M., and Troemel, E.R. (2019). Antagonistic paralogs control a switch between growth and pathogen resistance in C. elegans. PLoS Pathog. *15*, e1007528. https://doi.org/10.1371/journal.ppat.1007528.
12. Lazetic, V., Blanchard, M.J., Bui, T., and Troemel, E.R. (2023). Multiple pals gene modules control a balance between immunity and development in Caenorhabditis elegans. PLoS Pathog. *19*, e1011120. https://doi.org/10.1371/journal.ppat.1011120.
13. Sowa, J.N., Jiang, H., Somasundaram, L., Tecle, E., Xu, G., Wang, D., and Troemel, E.R. (2020). The Caenorhabditis elegans RIG-I Homolog DRH-1 Mediates the Intracellular Pathogen Response upon Viral Infection. J. Virol. *94*, e01173-19. https://doi.org/10.1128/JVI.01173-19.
14. Gang, S.S., Grover, M., Reddy, K.C., Raman, D., Chang, Y.T., Ekiert, D.C., Barkoulas, M., and Troemel, E.R. (2022). A pals-25 gain-of-function allele triggers systemic resistance against natural pathogens of C. elegans. PLoS Genet. *18*, e1010314. https://doi.org/10.1371/journal.pgen.1010314.
15. Chua, S.M., and Fraser, J.A. (2020). Surveying purine biosynthesis across the domains of life unveils promising drug targets in pathogens. Immunol. Cell Biol. *98*, 819–831. https://doi.org/10.1111/imcb.12389.
16. de Reuver, R., and Maelfait, J. (2024). Novel insights into double-stranded RNA-mediated immunopathology. Nat. Rev. Immunol. *24*, 235–249. https://doi.org/10.1038/s41577-023-00940-3.
17. Dhanwani, R., Takahashi, M., Mathews, I.T., Lenzi, C., Romanov, A., Watrous, J.D., Pieters, B., Hedrick, C.C., Benedict, C.A., Linden, J., et al. (2020). Cellular sensing of extracellular purine nucleosides triggers an innate IFN-beta response. Sci. Adv. *6*, eaba3688. https://doi.org/10.1126/sciadv.aba3688.
18. Sharma, V., Deo, P., and Sharma, A. (2023). Deficiency of adenosine deaminase 2 (DADA2): Review. Best Pract. Res. Clin. Rheumatol. *37*, 101844. https://doi.org/10.1016/j.berh.2023.101844.
19. Demirdag, Y., Fuleihan, R., Orange, J.S., and Yu, J.E. (2021). New primary immunodeficiencies 2021 context and future. Curr. Opin. Pediatr. *33*, 657–675. https://doi.org/10.1097/MOP.0000000000001075.
20. Grunebaum, E., Cohen, A., and Roifman, C.M. (2013). Recent advances in understanding and managing adenosine deaminase and purine nucleoside phosphorylase deficiencies. Curr. Opin. Allergy Clin. Immunol. *13*, 630–638. https://doi.org/10.1097/ACI.0000000000000006.
21. Whitmore, K.V., and Gaspar, H.B. (2016). Adenosine Deaminase Deficiency - More Than Just an Immunodeficiency. Front. Immunol. *7*, 314. https://doi.org/10.3389/fimmu.2016.00314.
22. Tecle, E., Chhan, C.B., Franklin, L., Underwood, R.S., Hanna-Rose, W., and Troemel, E.R. (2021). The purine nucleoside phosphorylase pnp-1 regulates epithelial cell resistance to infection in C. elegans. PLoS Pathog. *17*, e1009350. https://doi.org/10.1371/journal.ppat.1009350.

23. Bakowski, M.A., Desjardins, C.A., Smelkinson, M.G., Dunbar, T.L., Lopez-Moyado, I.F., Rifkin, S.A., Cuomo, C.A., and Troemel, E.R. (2014). Ubiquitin-mediated response to microsporidia and virus infection in C. elegans. PLoS Pathog. *10*, e1004200. https://doi.org/10.1371/journal.ppat.1004200.

24. Lazetic, V., Wu, F., Cohen, L.B., Reddy, K.C., Chang, Y.T., Gang, S.S., Bhabha, G., and Troemel, E.R. (2022). The transcription factor ZIP-1 promotes resistance to intracellular infection in Caenorhabditis elegans. Nat. Commun. *13*, 17. https://doi.org/10.1038/s41467-021-27621-w.

25. Pontarin, G., Ferraro, P., Bee, L., Reichard, P., and Bianchi, V. (2012). Mammalian ribonucleotide reductase subunit p53R2 is required for mitochondrial DNA replication and DNA repair in quiescent cells. Proc. Natl. Acad. Sci. USA *109*, 13302–13307. https://doi.org/10.1073/pnas.1211289109.

26. Ferraro, P., Franzolin, E., Pontarin, G., Reichard, P., and Bianchi, V. (2010). Quantitation of cellular deoxynucleoside triphosphates. Nucleic Acids Res. *38*, e85. https://doi.org/10.1093/nar/gkp1141.

27. McReynolds, M.R., Wang, W., Holleran, L.M., and Hanna-Rose, W. (2017). Uridine monophosphate synthetase enables eukaryotic de novo NAD(+) biosynthesis from quinolinic acid. J. Biol. Chem. *292*, 11147–11153. https://doi.org/10.1074/jbc.C117.795344.

28. Chi, C., Ronai, D., Than, M.T., Walker, C.J., Sewell, A.K., and Han, M. (2016). Nucleotide levels regulate germline proliferation through modulating GLP-1/Notch signaling in C. elegans. Genes Dev. *30*, 307–320. https://doi.org/10.1101/gad.275107.115.

29. Greene, B.L., Kang, G., Cui, C., Bennati, M., Nocera, D.G., Drennan, C.L., and Stubbe, J. (2020). Ribonucleotide Reductases: Structure, Chemistry, and Metabolism Suggest New Therapeutic Targets. Annu. Rev. Biochem. *89*, 45–75. https://doi.org/10.1146/annurev-biochem-013118-111843.

30. Wisitpitthaya, S., Zhao, Y., Long, M.J.C., Li, M., Fletcher, E.A., Blessing, W.A., Weiss, R.S., and Aye, Y. (2016). Cladribine and Fludarabine Nucleotides Induce Distinct Hexamers Defining a Common Mode of Reversible RNR Inhibition. ACS Chem. Biol. *11*, 2021–2032. https://doi.org/10.1021/acschembio.6b00303.

31. Felix, M.A., and Wang, D. (2019). Natural Viruses of Caenorhabditis Nematodes. Annu. Rev. Genet. *53*, 313–326. https://doi.org/10.1146/annurev-genet-112618-043756.

32. Tecle, E., and Troemel, E.R. (2022). Insights from C. elegans into Microsporidia Biology and Host-Pathogen Relationships. Exp. Suppl. *114*, 115–136. https://doi.org/10.1007/978-3-030-93306-7_5.

33. Balla, K.M., Andersen, E.C., Kruglyak, L., and Troemel, E.R. (2015). A wild C. elegans strain has enhanced epithelial immunity to a natural microsporidian parasite. PLoS Pathog. *11*, e1004583. https://doi.org/10.1371/journal.ppat.1004583.

34. McCarville, J.L., and Ayres, J.S. (2018). Disease tolerance: concept and mechanisms. Curr. Opin. Immunol. *50*, 88–93. https://doi.org/10.1016/j.coi.2017.12.003.

35. Troemel, E.R., Félix, M.A., Whiteman, N.K., Barrière, A., and Ausubel, F.M. (2008). Microsporidia are natural intracellular parasites of the nematode Caenorhabditis elegans. PLoS Biol. *6*, 2736–2752. https://doi.org/10.1371/journal.pbio.0060309.

36. Cali, A., Kotler, D.P., and Orenstein, J.M. (1993). Septata intestinalis N. G., N. Sp., an intestinal microsporidian associated with chronic diarrhea and dissemination in AIDS patients. J. Eukaryot. Microbiol. *40*, 101–112. https://doi.org/10.1111/j.1550-7408.1993.tb04889.x.

37. Antao, N.V., Lam, C., Davydov, A., Riggi, M., Sall, J., Petzold, C., Liang, F.X., Iwasa, J.H., Ekiert, D.C., and Bhabha, G. (2023). 3D reconstructions of parasite development and the intracellular niche of the microsporidian pathogen Encephalitozoon intestinalis. Nat. Commun. *14*, 7662. https://doi.org/10.1038/s41467-023-43215-0.

38. Watts, J.S., Harrison, H.F., Omi, S., Guenthers, Q., Dalelio, J., Pujol, N., and Watts, J.L. (2020). New Strains for Tissue-Specific RNAi Studies in Caenorhabditis elegans. G3 (Bethesda) *10*, 4167–4176. https://doi.org/10.1534/g3.120.401749.

39. Reddy, K.C., Dror, T., Sowa, J.N., Panek, J., Chen, K., Lim, E.S., Wang, D., and Troemel, E.R. (2017). An Intracellular Pathogen Response Pathway Promotes Proteostasis in C. elegans. Curr. Biol. *27*, 3544–3553.e5. https://doi.org/10.1016/j.cub.2017.10.009.

40. Wouters, M., Ehlers, L., Dzhus, M., Kienapfel, V., Bucciol, G., Delafontaine, S., Hombrouck, A., Pillay, B., Moens, L., and Meyts, I. (2024). Human ADA2 Deficiency: Ten Years Later. Curr. Allergy Asthma Rep. *24*, 477–484. https://doi.org/10.1007/s11882-024-01163-9.

41. Sarov, M., Murray, J.I., Schanze, K., Pozniakovski, A., Niu, W., Angermann, K., Hasse, S., Rupprecht, M., Vinis, E., Tinney, M., et al. (2012). A genome-scale resource for in vivo tag-based protein function exploration in C. elegans. Cell *150*, 855–866. https://doi.org/10.1016/j.cell.2012.08.001.

42. Zhang, T., Noll, S.E., Peng, J.T., Klair, A., Tripka, A., Stutzman, N., Cheng, C., Zare, R.N., and Dickinson, A.J. (2023). Chemical imaging reveals diverse functions of tricarboxylic acid metabolites in root growth and development. Nat. Commun. *14*, 2567. https://doi.org/10.1038/s41467-023-38150-z.

43. Dean, P., Hirt, R.P., and Embley, T.M. (2016). Microsporidia: Why Make Nucleotides if You Can Steal Them? PLoS Pathog. *12*, e1005870. https://doi.org/10.1371/journal.ppat.1005870.

44. Saka, H.A., and Valdivia, R.H. (2010). Acquisition of nutrients by Chlamydiae: unique challenges of living in an intracellular compartment. Curr. Opin. Microbiol. *13*, 4–10. https://doi.org/10.1016/j.mib.2009.11.002.

45. Greiner-Tollersrud, O.K., Krausz, M., Boehler, V., Polyzou, A., Seidl, M., Spahiu, A., Abdullah, Z., Andryka-Cegielski, K., Dominick, F.I., Huebscher, K., et al. (2024). ADA2 is a lysosomal deoxyadenosine deaminase acting on DNA involved in regulating TLR9-mediated immune sensing of DNA. Cell Rep. *43*, 114899. https://doi.org/10.1016/j.celrep.2024.114899.

46. Kim, S., Ramalho, T.R., and Haynes, C.M. (2024). Regulation of proteostasis and innate immunity via mitochondria-nuclear communication. J. Cell Biol. *223*, e202310005. https://doi.org/10.1083/jcb.202310005.

47. Tao, G., Liao, W., Hou, J., Jiang, X., Deng, X., Chen, G., and Ding, C. (2024). Advances in crosstalk among innate immune pathways activated by mitochondrial DNA. Heliyon *10*, e24029. https://doi.org/10.1016/j.heliyon.2024.e24029.

48. Zavialov, A.V., Yu, X., Spillmann, D., Lauvau, G., and Zavialov, A.V. (2010). Structural basis for the growth factor activity of human adenosine deaminase ADA2. J. Biol. Chem. *285*, 12367–12377. https://doi.org/10.1074/jbc.M109.083527.

49. Kohn, D.B. (2024). Gene therapy for adenosine deaminase severe combined immune deficiency-An unexpected journey of four decades. Immunol. Rev. *322*, 148–156. https://doi.org/10.1111/imr.13293.

50. Brenner, S. (1974). The genetics of Caenorhabditis elegans. Genetics *77*, 71–94. https://doi.org/10.1093/genetics/77.1.71.

51. Stiernagle, T. (2006). Maintenance of C. elegans (WormBook), pp. 1–11. https://doi.org/10.1895/wormbook.1.101.1.

52. Kamath, R.S., Martinez-Campos, M., Zipperlen, P., Fraser, A.G., and Ahringer, J. (2001). Effectiveness of specific RNA-mediated interference through ingested double-stranded RNA in Caenorhabditis elegans. Genome Biol. *2*, RESEARCH0002. https://doi.org/10.1186/gb-2000-2-1-research0002.

53. Paix, A., Folkmann, A., Rasoloson, D., and Seydoux, G. (2015). High Efficiency, Homology-Directed Genome Editing in Caenorhabditis elegans Using CRISPR-Cas9 Ribonucleoprotein Complexes. Genetics *201*, 47–54. https://doi.org/10.1534/genetics.115.179382.

54. Arribere, J.A., Bell, R.T., Fu, B.X.H., Artiles, K.L., Hartman, P.S., and Fire, A.Z. (2014). Efficient marker-free recovery of custom genetic modifications with CRISPR/Cas9 in Caenorhabditis elegans. Genetics *198*, 837–846. https://doi.org/10.1534/genetics.114.169730.

55. Subramanian, A., Tamayo, P., Mootha, V.K., Mukherjee, S., Ebert, B.L., Gillette, M.A., Paulovich, A., Pomeroy, S.L., Golub, T.R., Lander, E.S., and Mesirov, J.P. (2005). Gene set enrichment analysis: a knowledge-based approach for interpreting genome-wide expression profiles. Proc.

Natl. Acad. Sci. USA *102*, 15545–15550. https://doi.org/10.1073/pnas.0506580102.

56. Hulsen, T., de Vlieg, J., and Alkema, W. (2008). BioVenn - a web application for the comparison and visualization of biological lists using area-proportional Venn diagrams. BMC Genom. *9*, 488. https://doi.org/10.1186/1471-2164-9-488.

57. Rivera, D.E., Lazetic, V., Troemel, E.R., and Luallen, R.J. (2022). RNA Fluorescence in situ Hybridization (FISH) to Visualize Microbial Colonization and Infection in Caenorhabditis elegans Intestines. J. Vis. Exp. https://doi.org/10.3791/63980.

58. Batachari, L.E., Dai, A.Y., and Troemel, E.R. (2024). Caenorhabditis elegans RIG-I-like receptor DRH-1 signals via CARDs to activate antiviral immunity in intestinal cells. Proc. Natl. Acad. Sci. USA *121*, e2402126121. https://doi.org/10.1073/pnas.2402126121.

59. Batachari, L.E., Sarmiento, M.B., Wernet, N., and Troemel, E.R. (2024). Orsay Virus Infection in Caenorhabditis elegans. Curr. Protoc. *4*, e1098. https://doi.org/10.1002/cpz1.1098.

60. Madeira, F., Pearce, M., Tivey, A.R.N., Basutkar, P., Lee, J., Edbali, O., Madhusoodanan, N., Kolesnikov, A., and Lopez, R. (2022). Search and sequence analysis tools services from EMBL-EBI in 2022. Nucleic Acids Res. *50*, W276–W279. https://doi.org/10.1093/nar/gkac240.

61. Waterhouse, A.M., Procter, J.B., Martin, D.M.A., Clamp, M., and Barton, G.J. (2009). Jalview Version 2--a multiple sequence alignment editor and analysis workbench. Bioinformatics *25*, 1189–1191. https://doi.org/10.1093/bioinformatics/btp033.

STAR★METHODS

KEY RESOURCES TABLE

REAGENT or RESOURCE	SOURCE	IDENTIFIER
Antibodies		
Orsay RNA1 Cal Fluor Red 610 (CF610)	Biosearch Technologies	N/A
Rosay RNA1 Quasar 670 (Q670)	Biosearch Technologies	N/A
Orsay RNA2 Cal Fluor Red 610 (CF610)	Biosearch Technologies	N/A
Orsay RNA2 Quasar 670 (Q670)	Biosearch Technologies	N/A
MicroB Red	Biosearch Technologies	N/A
MicroB Green	Biosearch Technologies	N/A
Ultra-LEAF™ Purified anti-mouse IFNAR-1 Antibody	BioLegend	clone MAR1-5A3; cat#127322; RRID AB_11149116
E. intestinalis 16S rRNA FISH probe Quasar 570	LGC Biosearch Technologies	Antao et al.[37]
Bacterial and virus strains		
E. coli: OP50-1	Gary Ruvkun lab	N/A
OP50 RNAi	Meng Wang lab	
E. coli: HT115	Gary Ruvkun lab	
Virus: Orsay Virus	Felix et al., 2011	
N parisii	Troemel et al., 2008	
Chemicals, peptides, and recombinant proteins		
Deoxyadenosine	Sigma	cat#D7400
Deoxyinosine	Thermo Fisher Scientific	cat#H52292.06
Hypoxanthine	Sigma	cat#H9636
Inosine	Sigma	cat#I4125
Adenosine	Sigma	cat#A9251
Fludarabine	*Selleckchem*	*cat*#S1491
TRI reagent	Molecular Research Center, Inc	*cat*#TR118
1-Bromo-3-chloropropane	BCP, Molecular Research Center, Inc	*cat*#BP151
Fluorescent beads	Fluoresbrite Polychromatic Red Microspheres, Polysciences Inc.	*cat*#19507-5
2′-Deoxyadenosine monohydrate for cell culture studies	Sigma Aldrich	*cat*# D7400
Deposited data		
RNAseq of *adah-1/pnp-1* RNAi treatment	This study	GEO: GSE262563
RNAseq of used for GSEA: IPR UP	Reddy et al. 2019	GEO: GSE118400
RNAseq of used for GSEA: PALS-22 UP	Reddy et al. 2019	GEO: GSE118400
RNAseq of used for GSEA: PNP-1 UP	Tecle et al. 2021	GEO: GSE165786
Metabolomics of *adah-1* RNAi and *pnp-1* mutants	This study	NMDR Project ID: PR002285
Experimental models: Cell lines		
E. intestinalis	ATCC	ATCC 50506
Human umbilical vein endothelial cells (HUVEC)	ATCC	ATCC PCS-100-010
Vero monkey kidney cells	ATCC	ATCC CCL-81
Experimental models: Organisms/strains		
C. elegans: Strain N2 wild-type	Caenorhabditis Genetics Center	N2

(*Continued on next page*)

Continued

REAGENT or RESOURCE	SOURCE	IDENTIFIER
C. elegans: Strain ERT054 *jyIs8[pals-5p::GFP, myo-2::mCherry] X*	This study	ERT054
C. elegans: Strain ERT1095 *adah-1(jy125)/+IV; jyIs8 X*	This study	ERT1095
C. elegans: Strain ERT1096*: adah-1(jy125)/+IV; jyIs8 X; nT1[qIs51](IV;V)*	This study	ERT1096
C. elegans: Strain ERT1200 *jyEx316[adah-1p::adah-1::mScarlet::3xHA; gcy-8p::GFP]*	This study	ERT1200
C. elegans: Strain ERT1215 *frSi17[mtl-2p::rde-1 3′UTR] II; rde-1(ne300) V; jyIs8 X*	This study	ERT1215
C. elegans: Strain ERT1216 *frSi21[col-62p::rde-1 3′UTR] II, rde-1(ne300) V, jyIs8 X*	This study	ERT1216
C. elegans: Strain ERT1260 *jyEx316[adah-1p::adah-1::mScarlet::3xHA; gcy-8p::GFP]; C06G3.5(jy125))/nT1[qIs51]IV; jyIs8 X*	This study	ERT1260
C. elegans: Strain ERT1265 *frSi17 [mtl-2p::rde-1 3′UTR] II; rde-1(ne300)V*	This study	ERT1265
C. elegans: Strain ERT1266 *frSi21 [col-62p::rde-1 3′UTR] II, rde-1(ne300)V,*	This study	ERT1266
C. elegans: Strain ERT1281 *otIs45[punc-119::GFP] V, jyEx316[adah-1p::adah-1::mScarlet::3xHA; gcy-8p::GFP]*	This study	ERT1281
C. elegans: Strain ERT1282 *unc-119(ed3) III; jySi24[myo-3p::GFP::APX_NES::unc-54; unc-119(+)] II; jyEx316[adah-1p::adah-1::mScarlet::3xHA; gcy-8p::GFP]*	This study	ERT1282
C. elegans: Strain ERT1349 *unc-119(ed3) III; jySi25[pET595: dpy-7p::GFP::APX_NES::unc-54; unc-119(+)] II; jyEx316[(pET771) adah-1p::adah-1::mScarlet::3xHA; gcy-8p::GFP]*	This study	ERT1349
C. elegans: Strain ERT485 *pnp-1(jy90)IV*	Tecle et al. 2021	ERT485
C. elegans: Strain ERT588 *zip-1(jy13) III; jyIs8 X*	Lažetić et al. 2022	ERT588
C. elegans: Strain ERT797 *jyIs8 X; C06G3.5(jy125)/+ IV*	This study	ERT797
C. elegans: Strain ERT889 *zip-1(jy14); jyIs8 X*	Lažetić et al. 2022	ERT889
C. elegans: Strain VC1874 *mes-4(ok2326) V/nT1[qIs51] IV;V*	Caenorhabditis Genetics Center	VC1874
C. elegans: Strain WM27 *rde-1(ne219) V*	Caenorhabditis Genetics Center	WM27
C. elegans: Strain WM45 *rde-1(ne300) V*	Caenorhabditis Genetics Center	WM45
C. elegans: Strain IG1839 *frSi17 [mtl-2p::rde-1 3′UTR] II. frIs7 [nlp-29p::GFP + col-12p::dsRed] IV*	Caenorhabditis Genetics Center	IG1839
C. elegans: Strain IG1846 *frSi21 [col-62p::rde-1 3′UTR] II; frIs7 [nlp-29p::GFP + col-12p::dsRed] IV*	Caenorhabditis Genetics Center	IG1846
C. elegans: Strain ERT1259 *rde-1(ne300) V*	This study; backcrossed WM45	ERT1259
C. elegans: Strain ERT878 *pnp-1(jy121) IV*	Tecle et al. 2021	ERT878
C. elegans: Strain DA465 *eat-2(ad465) II*	Gary Ruvkun laboratory	DA465
C. elegans: Strain ERT1322 *drh-3(ne4253) I; drh-1(jy110) IV; jyIs8 X*	This study	ERT1322

(*Continued on next page*)

Continued

REAGENT or RESOURCE	SOURCE	IDENTIFIER
C. elegans: Strain ERT1325 *jyEx366[vha-6p::adah-1::mScarlet::3xHA; gcy-8p::GFP]*	This study	ERT1325
C. elegans: Strain ERT1345 *jyEx366[vha-6p::adah-1::mScarlet::3xHA; gcy-8p::GFP]; C06G3.5(jy125)IV; jyIs8 X*	This study	ERT1345
C. elegans: Strain ERT1351 *jyEx376[dpy-7p::adah-1::mScarlet::3xHA; gcy-8p::GFP]; C06G3.5(jy125)I; jyIs8 X*	This study	ERT1351
C. elegans: Strain ERT1350 *jyEx376[dpy-7p::adah-1::mScarlet::3xHA; gcy-8p::GFP]*	This study	ERT1350
C. elegans: Strain ERT1347 *pnp-1(jy90) drh-1(jy110); jyIs8; drh-3(ne4253) I*	This study	ERT1347
C. elegans: Strain ERT356 *pals-22(jy1) III*	Reddy et al. 2019	ERT356
Oligonucleotides		
See Table S1 for oligonucleotide sequences used in this study		
Recombinant DNA		
RNAi clone: pL4440-RNAi control (OP50)	Ahringer RNAi Library	N/A
RNAi clone: pL4440-*unc-22* (OP50)	Ahringer RNAi Library	N/A
RNAi clone: pL4440-RNAi control (HT115)	Ahringer RNAi Library	N/A
RNAi clone: pL4440-*unc-22* (HT115)	Ahringer RNAi Library	N/A
RNAi clone: *Y10G11A1*	This study	N/A
RNAi clone: *C06G3.5(adah-1)*	Ahringer RNAi Library	N/A
RNAi clone: *pnp-1*	Ahringer RNAi Library	N/A
RNAi clone: *hprt-1*	This study	N/A
RNAi clone: *adss-1*	Ahringer RNAi Library	N/A
RNAi clone: *adsl-1*	Ahringer RNAi Library	N/A
RNAi clone: *T22D1.3*		N/A
RNAi clone: *gmps-1*	Ahringer RNAi Library	N/A
Plasmid: pET771	This study	N/A
Plasmid: pET772	This study	N/A
Plasmid: pET774	This study	N/A
Software and algorithms		
FIJI ImageJ 2.14.0	NIH Image	RRID:SCR_003070
GraphPad Prism 10	GraphPad Software, Inc.	RRID:SCR_002798
ZEISS ZEN Microscopy Software	Carl Zeiss AG	RRID:SCR_013672
Gene Set Enrichment Analysis (GSEA) v3.0 software	Subramanian et al. 2005	RRID:SCR_003199
BioVenn	Hulsen et al. 2008	https://doi.org/10.1186/1471-2164-9-488
Morpheus		RRID:SCR_017386; https://software.broadinstitute.org/morpheus
Jalview 2.11.2.3.	Waterhouse et al. 2009	N/A; https://doi.org/10.1093/bioinformatics/btp033
Other		
DRAQ5	Novus Biologicals	NBP2-81125
Calcofluor white	Sigma Aldrich	18909

EXPERIMENTAL MODEL AND STUDY PARTICIPANT DETAILS

C. elegans strains were maintained at 20°C on NGM plates seeded with *E. coli* OP50-1[50,51] unless otherwise noted. Worms were synchronized by subjecting gravid adults to a bleaching solution (800 μL of 5.65–6% sodium hypochlorite solution and 200 μL of

2 M NaOH) and collecting the eggs, which were incubated in M9 at 20°C under continuous rotation for 20-24 h to hatch into synchronized, starved L1s. All strains used in this study are listed in Table S1.

Vero monkey kidney cells (ATCC CCL-81) were used to generate spores of *E. intestinalis*, and Human umbilical vein endothelial cells (HUVEC) (ATCC PCS-100-010) were purchased from ATCC specifically for the infection assays described below.

See key resources table for more information on *C. elegans* strains and cell lines.

METHOD DETAILS

RNAi screen of the purine salvage pathway

To choose purine salvage enzymes for RNAi analysis, we used the KEGG pathway annotation for purine salvage metabolism in *C. elegans* (https://www.kegg.jp/pathway/cel00230). Altogether eight genes were tested: *Y10G11A1, C06G3.5 (*which we named *adah-1), pnp-1 (*our positive control), *hprt-1, adss-1, adsl-1, T22D1.3,* and *gmps-1* (Figure S1). Because RNAi clones were not available for *Y10G11A.1* and *hprt-1*, we generated them by Gibson cloning of 292 bp of the cDNA sequence of exon 3 from *Y10G11A.1* and 439 bp of exon 3 for *hprt-1* into the L4440 RNAi vector. All other RNAi clones were obtained from the Ahringer or Vidal RNAi libraries. All constructs were in *E. coli* strain HT115 and were sequence verified. Three independent RNAi plates were tested for each RNAi clone in each experiment, with three to five L4 *jyIs8[pals-5p::GFP]* animals added to each plate. These *jyIs8[pals-5p::GFP]* animals were incubated at 20°C and produced progeny, which were then monitored for *pals-5p::gfp* expression daily until they reached adulthood. 50 F1 animals were scored for *pals-5p::gfp* expression at each timepoint in each experiment. Here, only RNAi against *pnp-1* and *adah-1* caused increased *pals-5p::GFP* expression compared to control. Two independent experimental replicates were performed (each with three plates).

RNAi treatment

RNA interference was performed using the feeding method by plating overnight cultures of *E. coli* HT115 or OP50-1 on NGM plates supplemented with 5 mM IPTG and 1 mM carbenicillin followed by incubation at room temperature for 3–4 days[52] Animals were transferred to these plates and incubated at 20°C for varying numbers of generations and times, as described in more detail below for various experiments. The empty vector L4440 was used as a negative control. *unc-22* RNAi was used as a positive control for efficacy of RNAi.

CRISPR/Cas9-mediated generation of *adah-1(jy125)* mutant, and strain construction with nT1 balancer

A *dpy-10* co-CRISPR method was used to monitor for deletion of the *adah-1* locus.[53,54] Specifically two crRNAs were used, one targeting the 5′ end (CGTGTTTTGCTCATGCTTGT) and the other the 3′ end of the *adah-1* gene (GAGTACAATTATCGACACTG). *dpy-10* crRNA was used as a control. All crRNA were ordered from IDT and resuspended to 100 μM. 0.5 μL of each crRNA was mixed with 2.5 μl of 100 μM tracer RNA; 1.5 μL of this mix was complexed to 3.5 μL of 40 μM purified Cas9-NLS protein ordered from QB3 Berkeley. Injections were performed into *jyIs8[pals-5p::GFP]* to monitor for GFP induction in candidate CRISPR-deleted animals. Dumpy and/or GFP-positive F1 animals were submitted to genotyping with the primers listed in Table S1.

The CRISPR-generated strain ERT797 *adah-1(jy125); jyIs8* mutant was back-crossed twice with the N2 strain, which removed the *dpy-10* co-CRISPR mutation, and created strain ERT1095, which, together with ERT1096 (see below) was analyzed for correlation between *pals-5p::GFP* expression and genotype, as shown in Figure S2. This backcrossed strained was then crossed to VC1874 *mes-4(ok2326) V/nT1 [qIs51] IV;V* to generate the balanced heterozygous strain ERT1096 *adah-1(jy125) IV/nT1 [qIs51] IV;V*; *jyIs8 X*, which is shown in Figure 1. Progeny showing both pharyngeal mCherry and GFP signal were genotyped for *jy125* using the primers listed in Table S1.

Generation of transgenic strains

To localize *adah-1* expression, the construct pET771 *adah-1p::adah-1::mScarlet::3xHA* was generated as follows: the *adah-1* promoter region (1.4 kb upstream of *adah-1*) and the *adah-1a* cDNA sequence were ordered as gene blocks from IDT and assembled into a vector containing *C. elegans* codon-optimized mScarlet (wrmScarlet referred to as mScarlet in the text), 3X HA tag and the *unc-54* UTR to create a C-terminal fusion using the NEBuilder Hifi DNA Assembly kit (NEB*).* The resulting pET771 construct was injected at 7.5 ng/μL together with 20 ng/μL of co-injection marker *gcy-8::GFP* in a total of 100 ng/μL, which generated *C. elegans* strain ERT1200 *jyEx316 [pET771(adah-1p::adah-1::mScarlet::3xHA)]; gcy-8p::GFP]*.

To rescue *adah-1(jy125/jy125)* mutant phenotypes, the *jyEx316* array from strain ERT1200 was crossed into strain ERT1096 *adah-1(jy125)/nT1 [qIs51]*; *jyIs8* to generate ERT1260 *adah-1(jy125)/nT1[qIs51]*; *jyIs8; jyEx316*.

To generate the tissue-specific rescue strains, worms expressing *adah-1* specifically in the intestine or the epidermis were generated by replacing the *adah-1* promoter sequence with the *vha-6* promotor region (intestinal expression) or the *dpy-7* promoter region (epidermal expression), respectively, in pET771 using the NEBuilder Hifi DNA Assembly kit (NEB*).* The resulting plasmids pET774 (intestine) and pET772 (Epidermis) were injected into N2 animals at 7.5 ng/μL together with 20 ng/μL of co-injection marker *gcy-8::GFP* in a total of 100 ng/μL, generating *C. elegans* strains ERT1325 (*jyEx366*) and ERT1350 *(jyEx376).* These strains were crossed with ERT1260 worms and then genotyped for the presence of *jyEx366* or *jzEx376*, respectively, and the absence of *jyEx316*. This process generated the strains ERT1351 (*jyEx376*) and ERT1345 (*jzEx366*).

To analyze ADAH-1:mScarlet expression through co-localization with known markers for different tissues, strain ERT1200 was crossed with OH441 *otIs45[uncp-119::GFP] V (pan-neuronal)*, ERT466 *jySi25[pET595: dpy-7p::GFP::APX_NES::unc-54; unc-119(+)] II* (epidermal), and ERT445 *unc-119(ed3) III; jySi24[pET594: myo-3p::GFP::APX_NES::unc-54; unc-119(+)] II* (muscle) to generate ERT1281, ERT1349, and ERT1282 respectively. For tissue-specific RNAi experiments, WM45, IG1839, and IG1846 were provided by CGC and backcrossed into N2 to generate ERT1259, ERT1265, and ERT1266, respectively. Crossing IG1839, and IG1846 with ERT054 *jyIs8* resulted in ERT1215, and ERT1216 respectively for tissue-specific RNAi reporter analysis. To analyze *pals-5p::GFP* expression in a *drh-1: drh-3* double mutant in *pnp-1* mutant background ERT781 was crossed with ERT792 to generate a *drh-1(jy110): drh-3(ne4253)* double mutant (ERT1323). ERT1323 was then crossed with ERT1049 to generate ERT1347 *pnp-1(jy90) drh-1(jy110); jyIs8; drh-3(ne4253).* See Table S1 for more details.

Imaging of *C. elegans*

To image animals on either a Zeiss Axio Imager M1 or a Zeiss LSM700 confocal microscope (Carl Zeiss, Thornwood, NY), they were mounted and anesthetized with 100 mM levamisole in M9 buffer on 5% agarose pads. Exposure times were adjusted to eliminate signal from *C. elegans* autofluorescence.

Pals-5p::GFP expression measurements

Measurements of *pals-5::GFP* levels in Figure 1I, 4A, 4B, 4F, 4E, 6B, 6E, S2A, S2E, S3A, S3B, and S3C, were performed by imaging animals using the ImageXpress Nano plate reader (Molecular Devices, LLC), followed by image analysis in FIJI. Mean gray value (ratio of integrated density and analyzed area) was measured for each animal and normalized to the background fluorescence. The experiments were performed in three biological replicates measuring fluorescence of at least 50 worms per replicate.

To measure *pals-5::GFP* fluorescence in the balanced *jy125* mutant strain ERT1096 *adah-1(jy125) IV/nT1 [qIs51] IV;V*; *jyIs8 X* compared to the *adah-1*::mScarlet overexpressing worms of ERT1260 *adah-1(jy125)/nT1[qIs51]*; *jyIs8; jyEx316* in Figure 1J, 30 gravid adult worms were picked onto 10 cm NGM plates seeded with *E. coli* OP50-1 to lay eggs for 4 h and then removed. L1 worms were collected in M9 buffer after 18 h and *pals-5::GFP* levels were quantified using the ImageXpress plate reader, followed by image analysis in FIJI.

Developmental rate assay

To determine the fraction of animals reaching the L4 stage as shown in Figure 1K, gravid adult worms were picked onto 10 cm NGM plates seeded with *E. coli* OP50-1 to lay eggs for 3 h at 20°C before removing the adult worms. For Figures 6E and S5C worms were picked onto 10 cm RNAi plates seeded with control RNAi, *adah-1* RNAi or *pnp-1* RNAi. These plates were incubated at 20°C to enable the eggs to hatch and develop into larvae, with the time course starting upon removal of the parents. 100 animals on each plate were scored for being at or older than the L4 stage at the 44 h, 64 h, and 72 h time points for Figures 1K and 6E and at the 44h time point for Figure S5C.

RNA extraction and qRT-PCR

For qRT-PCR analysis of IPR gene expression after RNAi treatment as shown in Figure 2A, ten *C. elegans* N2 at L4 stage (P0) were picked onto RNAi plates seeded with *adah-1*, *pnp-1*, or L4440 cultures in *E. coli HT115* background and incubated at 20°C until their progeny (F1) became gravid adults, which were bleached to obtain synchronized L1 progeny. 1500 L1 progeny (F2) were plated on two 10cm RNAi plates seeded with the respective RNAi culture. These animals were incubated at 20°C for 56 h, at which point animals were adults and collected for RNA extraction.

For qRT-PCR analysis of IPR gene expression upon deoxyadenosine supplementation as shown in Figure 4D, 4000 synchronized N2 L1 worms were grown on seeded 10 cm NGM plates for 48 h at 20°C until they developed into L4/adults. Next, 3000 of those animals were transferred to a 10 cm heat-killed OP50-1 plate supplemented with 30 mM deoxyadenosine and grown at 20°C for 24 h, at which point they were washed off the plates with M9 and collected for RNA extraction.

RNA was extracted using TRI reagent and 1-Bromo-3-chloropropane (BCP, Molecular Research Center, Inc.) followed by isopropanol precipitation and ethanol wash. The isolated RNA was converted to cDNA using the iScript (Bio-Rad) cDNA synthesis kit. qRT-PCR was performed using iQ SYBR green supermix (Bio-Rad) on a BioRad CFX Connect real-time system. Each biological replicate was performed in technical duplicates and normalized to *nhr-23* (Figure 2A) or *snb-1* (Figure 4E) control genes. Primers used for qRT-PCR are listed in Table S1.

RNAseq analysis

For RNAseq analysis of *pnp-1* and *adah-1* RNAi, animals were prepared identically as for qRT-PCR, except that after TRI-reagent extraction, the RNA was further purified using the RNeasy cleanup kit with gDNA Eliminator spin columns (Qiagen). All downstream steps related to sequencing were performed at the IGM Genomics Center, University of California, San Diego, La Jolla, CA. First, RNA quality was assessed using a TapeStation system, then sequencing libraries were constructed using the TruSeq stranded mRNA method followed by sequencing using run type SR75 on an Illumina HiSeq4000 sequencer (Illumina). RNA quality assessment and RNAseq were conducted. RNAseq reads will be publicly available upon publication at NCBI GEO database See key resources table for accession code.

Next, sequencing reads for *adah-1*, *pnp-1*, or L4440 samples were mapped to the *C. elegans* genome (Wormbase WS235 release) in Rstudio using Rsubread and then quantified using Featurecounts, with the Galaxy web platform (public server at https://usegalaxy.org/). Differential gene expression analysis was performed using limma-voom filtering out undetected and lowly expressed genes (CPM <1). An adjusted *p*-value of 0.05 and no fold-change cutoff was used to define differentially expressed genes.

Functional expression analysis

For functional expression analysis, Gene Set Enrichment Analysis v3.0 software was used.[55] Normalized RNAseq expression data was converted into a GSEA compatible filetype and then used for analysis. Independent GSEA analysis was performed for *adah-1* vs. L4440 and *pnp-1* vs. L4440 gene sets. For both analyses, a signal-to-noise metric with 1000 permutations was used. Heatmaps for the NES results were made using Morpheus (https://software.broadinstitute.org/morpheus/). Venn diagrams were generated with BioVenn.[56]

Targeted metabolomics

For *adah-1* RNAi analysis, six L4 stage N2 worms were picked onto 10 cm RNAi plates seeded with L4440 or *adah-1* in *E. coli HT115* overnight cultures grown at 37°C and incubated at 20°C. Gravid adult progeny were synchronized and 1500–2000 eggs were plated onto 10 cm RNAi plates seeded with the respective RNAi and incubated at 20°C for ~70 h. Six 10 cm RNAi plates were used for each condition per experiment. For analysis of the *pnp-1* mutant, synchronized N2 or *pnp-1(jy90)* L1 larvae were seeded onto 10 cm plates and kept at 20°C 4 days until they became adults, which were harvested, washed with M9 buffer, and transferred to 1.5 mL reaction tubes.[22] Approximately 100 μL of packed worms were collected and flash frozen in liquid nitrogen immediately. The samples were kept at −80°C until shipping. Metabolite extraction and LC-MS were performed with the Penn State Metabolomics Core facility.[22,27] Raw Data were processed with MS-DIAL and metabolite levels were corrected to chlorpropamide, an internal standard. Selected metabolites were determined by m/z and column retention time values of known standards. Eight independent experimental replicates were performed for each condition.

Dietary supplementation of purine metabolites

Purine-supplemented plates were made by adding the cell culture grade chemicals (Sigma) to NGM reagents prior to autoclaving the media. To test the role of different purines in Figure 4A, adenosine (Sigma cat. # A9251), 2′-deoxyadenosine (Sigma cat. #D7400), inosine (Sigma cat. #I4125), deoxyinosine (Thermo Fisher Scientific cat. #H52292.06) or hypoxanthine (Sigma cat. #H9636), respectively, was added at 30 mM. To perform a dose-response curve for deoxyadenosine in Figure 4B, deoxyadenosine was added at 1 mM, 3mM, 10 mM, 30 mM and 90 mM; 30 mM was used in all subsequent experiments. Purine-supplemented plates were seeded with 20X concentrated *E. coli* OP50-1 culture that was heat killed at 65°C for 30 min in 1 mL aliquots. For Figures 4A–4D, and Figures S3B and S3C, 3000 synchronized *jyIs8* and/or *jyIs8*; *zip-1, jyIs8*; *pnp-1(jy90), or jyIs8*; *drh-1/drh-3* L1 worms were grown on seeded 10 cm NGM plates for 48 h at 20°C. 300 L4/adult worms were transferred to a 6 cm dead OP50-1 plate supplemented with the specific concentration of purine metabolite and then grown at 20°C for 24 h. For Figure S3A 1200 synchronized *jyIs8* L1 worms were grown on seeded 10 cm control, *adah-1* or *pnp-1* RNAi plates for 48 h at 20°C and then transferred to 6 cm dead OP50-1 plates supplemented with 30 mM dAdo followed by incubation at 20°C for 24 h. Fluorescence measurements of *pals-5::GFP* were performed using the ImageXpress and analyzed in FIJI. Mean gray value was measured for each animal and normalized to the background fluorescence.

RNR inhibitor treatment

For Fludarabine treatment of pnp-1(jy90) animals in Figure 4F and 4G Fludarabine in DMSO (Selleckchem cat. #S1491) was plated on NGM plates seeded with E. coli OP50-1 at a final concentration of 50 μM. Control plates were prepared with DMSO. 300 synchronized L1 worms were grown on these plates for 4 days at 20°C. Worms were washed off the plates and fluorescence measurements of *pals-5::GFP* were performed with the ImageXpress and analyzed in FIJI. The mean gray value was measured for each animal and normalized to the background fluorescence.

Orsay Virus infection

Orsay virus filtrates were prepared by infecting RNAi-deficient animals and amplifying up the infected stock, followed by grinding and filtering.[23] To perform viral infections after RNAi (Figures 5A and 6C), about 1200 synchronized L1 larvae were added to a 10 cm NGM RNAi plate seeded with *adah-1*, *pnp-1*, or L4440 overnight cultures grown at 37°C for 15 h in *E. coli* OP50 background and incubated at 20°C. After plating, animals were incubated at 20°C for 44 h until the L4 stage, at which point they were top-plated with 900 μL of an infection mix comprised of 30 μL of 1:10 diluted virus filtrate, 150 μL of 10X OP50-1 bacteria, and 720 μL of M9 buffer. Plates were dried in the laminar flow hood at room temperature for 30 min and incubated at 20°C for 18 h. After infection, animals were collected for fixation and FISH staining, which was performed by fixing worms in 4% paraformaldehyde and incubating at 47°C overnight with two equally mixed FISH probes that hybridize to either Orsay RNA1 or RNA2 genome segments (Biosearch Technologies), both conjugated to the red Cal Fluor 610 fluorophore.[57]

For Orsay Virus infections after deoxyadenosine supplementation (Figure 5C), 3000 synchronized N2 L1 stage worms were grown on seeded 10 cm NGM plates for 48 h at 20°C, at which point 300 of the animals were transferred to a 6 cm NGM plate supplemented

with 30 mM deoxyadenosine and seeded with heat-killed OP50-1. These animals were incubated at 20°C for 24 h until they became young adults. Then 15 μL of Orsay virus filtrate in M9 buffer was mixed with heat-killed OP50-1 bacteria to a final volume of 300 μL, which was added to infect the adult worms on the plates. These plates were then dried in the laminar flow hood at room temperature for 30 min, incubated at 20°C for 18 h and then animals were collected for fixation and staining with *Orsay Virus* FISH probes as described above.

For viral infections of *adah-1*^{OE} animals compared to WT animals in Figure S4E 1000 synchronized L1 stage worms were grown on seeded 10 cm NGM plates for 44 h at 20°C. 10 μL of Orsay virus filtrate was mixed with 150 μL OP50-1 bacteria to a final volume of 1000 μL with M9 buffer, and plated on top of the L4 stage worms. The plates were then dried in the laminar flow hood at room temperature for 30 min, and then incubated at 20°C for 24 h. Animals were collected for fixation and staining with *Orsay Virus* FISH probes as described above.

To measure Orsay virus pathogen load, FISH probe mean fluorescence was determined by measuring mean gray value (ratio of integrated density and analyzed area) of each animal in FIJI and then normalizing to the background fluorescence upon imaging animals using a Zeiss Axio Imager M1 of the ImageXpress imager.[58,59]

N. parisii infection, pathogen load quantification and survival assays

N. parisii spores were prepared by infecting animals and amplifying up the infected stock, followed by grinding and filtering.[33] For *N. parisii* sporoplasm assays upon RNAi treatment (Figure 5B), ten adult worms were picked onto 10 cm RNAi plates seeded with *adah-1*, *pnp-1*, or L4440 in *E. coli* OP50 background grown at 37°C for 15 h and incubated at 20°C. Their gravid adult progeny were then bleached from 4 pooled plates to obtain synchronized L1 progeny (F2). 1200 synchronized L1 F2 progeny were mixed with 2.5 × 10^6 *N parisii* spores, 25 μL 10X concentrated OP50-1 bacteria and M9 to bring the total volume to 300 μL. This mixture was plated on room temperature unseeded 6 cm NGM plates, allowed to dry for 30 min and then incubated at 25°C for 3 h. Two plates were used per condition. For *N. parisii* infections of *adah-1*^{OE} animals compared to WT animals in Figure S4D 1200 synchronized L1 animals mixed with 2.5 × 10^6 *N parisii* spores, 25 μL 10X concentrated *E. coli* OP50-1 and brought to a total volume of 300 μL with M9 buffer. This mixture was plated on unseeded 6 cm NGM plates, allowed to dry for 30 min and then incubated at 25°C for 3 h. Two plates were used per condition.

Animals were fixed in 4% paraformaldehyde and then stained using a FISH probe specific to *N. parisii* ribosomal RNA conjugated to Cal Fluor 610 dye (Biosearch Technologies). For the 3 hpi timepoint, pathogen load was determined by counting sporoplasms per worm using the 40x objective on a Zeiss AxioImager M1 microscope.

For *N. parisii* infections after deoxyadenosine supplementation in Figure 5D, 3000 synchronized N2 L1 stage worms were grown on seeded 10 cm NGM plates for 48 h at 20°C until they were young adults. These animals were transferred to a 6 cm dead OP50-1 plate supplemented with 30 mM deoxyadenosine and incubated at 20°C for 24 h. Then these young adults were washed off the plates and pelleted in ~50 μL M9, mixed with 2 million *N. parisii* spores, heat killed OP50-1, and this mixture was plated on unseeded 6-cm NGM plates for pulse-infection of 3 h at 25°C. Infected worms were washed off the plates, transferred to fresh 6-cm 30 mM deoxyadenosine supplemented NGM plates seeded with heat-killed OP50-1 (and no *N. parisii*), and returned to 25°C for 30 h. Animals were fixed and incubated with *N. parisii* FISH probes as described above. Samples were analyzed for meronts on an ImageXpress imager. Worm outlines were traced using FIJI software (excluding the head regions) and average fluorescence intensity of each worm was quantified and background corrected.

For survival assays, adult worms were picked onto 10 cm RNAi plates seeded with *adah-1*, *pnp-1*, or L4440 in an *E. coli* OP50 background. Worms were incubated at 20°C for 4 days. Gravid F1s were then bleached to obtain synchronized L1 progeny (F2). Synchronized L1s were plated on seeded 6 cm RNAi plates and incubated at 20°C for 44 h. L4s were then washed off plates and resuspended in 100 μL M9 buffer. For *N. parisii* infections, worms were mixed with 50 μL 10X concentrated *E. coli* OP50-1, *N. parisii* spores, and brought up to a total volume of 300 μL. The entire 300 μL mixture was transferred onto unseeded NGM plates and dried in a laminar flow hood for 40 min. Plates were then incubated at 25°C for 3 h. Infected worms were washed off plates with M9, followed by three additional washes. Worms were then plated onto a fresh 6 cm RNAi plate. For each treatment condition, 40 worms were picked onto three 3.5 cm tissue culture-treated RNAi plates (120 total worms/treatment). Plates were incubated at 25°C and survival was measured every 24 h. When scoring worms, live worms were transferred to fresh RNAi plates until progeny production halted.

Bead feeding assay

For the bead feeding assay upon RNAi treatment in Figure S4C 1200 synchronized WT N2 and *eat-2* mutant worms were grown on empty vector RNAi, *adah-1* RNAi, or *pnp-1* RNAi plates for 44 h. L4 worms were washed off the plates and 400 animals were mixed with 4 μL fluorescent beads (Fluoresbrite Polychromatic Red Microspheres, Polysciences Inc.), 25 μL 10X concentrated OP50-1 *E coli*, and M9 (total volume 250 μl). For Figure S6B 1200 synchronized L1 worms were grown on seeded 10 cm NGM plates for 48 h at 20°C and then transferred to 6 cm dead OP50-1 plates supplemented with 30 mM dAdo. After incubation at 20°C for 24 h worms were washed off the plates and mixed with 4 μL fluorescent beads (Fluoresbrite Polychromatic Red Microspheres, Polysciences Inc.), 25 μL 10X concentrated heat-killed *E. coli* OP50-1, and M9 (total volume 250 μl). For both assays this mixture was then plated on 6 cm NGM plates, dried for 5 min and then incubated at 25°C for 5 min. Plates were then shifted to ice, worms washed with ice-cold PBST and fixed in 4% paraformaldehyde. Animals were imaged using ImageXpress. Fluorescence was analyzed in FIJI.

E. intestinalis infection and quantification

E. intestinalis (ATCC 50506) spores were propagated in Vero monkey kidney cells (ATCC CCL-81) grown in high-glucose DMEM (Gibco 11965092) supplemented with 10% fetal bovine serum (VWR 89510-188) and non-essential amino acids (Gibco 11140050).[37] Human umbilical vein endothelial cells (HUVEC; ATCC PCS-100-010) were grown in Lonza EGM-2 Endothelial cell growth medium (CC-3162) for fewer than 10 doublings. All cell lines were tested monthly for mycoplasma and were consistently negative.

HUVECs were seeded onto sterile glass coverslips treated with 1% porcine gelatin (Sigma Aldrich G1890). One or two days later, confluent cells were pre-treated for 24 h with 0 mM, 0.1 mM, 0.25 mM, 0.5 mM, 1 mM, or 2 mM deoxyadenosine; or 0 mM deoxyadenosine, 0.5 mM deoxyadenosine, or 0.5 mM deoxyadenosine with 10 μg/mL anti-IFNalphaR1 antibody. The media was then aspirated and replaced with *E. intestinalis* in EGM-2 lacking compounds at a MOI of 10–20, and parasites were allowed to invade host cells for 3 h. After the invasion period, the media was aspirated and replaced with the same concentration of deoxyadenosine or anti-IFNalphaR1 antibody used in the pre-treatment for 24 additional hours. Thus, over a 51 h experiment period, 48 h were under deoxyadenosine treatment. The coverslips were fixed in 4% paraformaldehyde in PBS for 15 min at room temperature, washed three times in PBS, and permeabilized for 30 min at room temperature with 0.25% Triton X-100 and 1% BSA in PBS. The coverslips were stained for 30 min at room temperature with 2 μg/μL calcofluor white (Sigma Aldrich 18909) and 0.5X DRAQ5 (Novus Biologicals NBP2-81125), washed three times with PBS, and were equilibrated for 5 min in FISH hybridization buffer (900 mM NaCl, 20 mM Tris HCl, 0.01% SDS). Staining with 125 nM Quasar 570 *E intestinalis* 16S rRNA probe (LGC Biosearch Technologies[37]; and https://doi.org/10.17504/protocols.io.3byl495wogo5/v1) was conducted overnight at 37°C. The coverslips were washed twice in FISH hybridization buffer with 5 mM EDTA, mounted with Prolong Diamond antifade (Thermo Fisher P36965), and dried for 30 min at 37°C. Imaging was conducted on a Zeiss AxioObserver microscope with a 20× air objective, Zeiss HXP metal halide lamp with dsRed, DAPI, and Cy5 filter set dichroics, and ORCA-Flash4.0 CMOS camera. The experiments were performed in biological triplicate. *E. intestinalis* infection was quantified as follows. Images were opened in FIJI. A region of interest (ROI) was drawn around contiguous regions of *E. intestinalis* FISH probe staining, which marks intracellular parasites. The areas of the ROIs were measured using the Measure tool in FIJI and were exported into Prism 10 and a Kruskal-Wallis test was used to calculate *p*-values.

Tissue-specific RNAi

For tissue specific RNAi analyses, 12-20 adult worms of the respective strain were picked onto three 10 cm NGM plates seeded with *E. coli* OP50-1. Gravid adult progeny from three pooled plates were bleached to obtain synchronized L1 progeny. 1200 synchronized L1 worms were plated on NGM RNAi plates seeded with *adah-1*, *pnp-1*, or L4440 control RNAi overnight cultures (in *E. coli* OP50 background) grown at 30°C for 19.5 h and incubated at 20°C for 3 days until the adult stage. Worms were washed off the plates with M9 buffer for analysis of *pals-5p::GFP* expression or subjected Orsay virus infection, as described above. Fluorescence measurements shown in Figure 6 C were performed using the COPAS Biosorter (Union Biometrica). Fluorescent signal of *pals-5p::*GFP was normalized to the TOF, as a proxy for worm length.

Multiple sequence alignment

The multiple sequence alignment in Figure S1 was calculated with Clustal Omega[60] and visualized using Jalview 2.11.2.3.[61] The sequences were derived from NCBI: *C. elegans* ADAH-1 isoforma A (isoA) GenBank: CCD83552.1 *C. elegans* ADAH-1 isoform B (isoB) GenBank: CCD83553.1, *Homo sapiens* ADA1 GenBank: NP_000013.2, *H. sapiens* ADA2 isoA GenBank: NP_001269154.1, *E. coli* adenosine deaminase GenBank: WP_327746800.1.

QUANTIFICATION AND STATISTICAL ANALYSIS

All performed data analysis and statistical analyses were performed in Prism 10 unless noted otherwise. Means with standard deviation error bars are presented unless otherwise noted. Details to the statistical tests and samples sizes are described in the respective figure legends.